Robust Hybrid Beamforming with Phased Antenna Arrays for Downlink SDMA in Indoor 60 GHz Channels

Sau-Hsuan Wu, Lin-Kai Chiu, Ko-Yen Lin, and Tsung-Hui Chang

***Abstract*—A hybrid architecture is presented for downlink beamforming (BF) with phased antenna arrays (PAA) in indoor 60 GHz spatial division multiple access (SDMA) channels. To manage the multiple access and inter-symbol interferences (MAI/ISI) encountered in SDMA with limited feedbacks, a cost-effective time-domain hybrid BF (HBF) method is presented to exploit the directivity provided by PAA in radio frequency (RF) beam patterns and the spatial diversity offered by multiple baseband processing modules. To maintain signal qualities under unpredictable MAI/ISI in wireless multimedia streaming to which indoor 60 GHz radio mainly applies, robust beamformers are designed to maintain the signal to interference-plus-noise ratio (SINR) for each user with minimum total transmit power. The percentages in which the target SINRs can be satisfied with the proposed HBF schemes are found sensitive to uncertainties in the phase shifters of PAA. Two kinds of robust formulations are thus proposed to jointly combat the MAI, ISI and phase uncertainties. Robust beamformers with semi closed-form expressions can be obtained with a nonlinear kind of them, whose SINR satisfaction ratio can attain 80% or more by extensive simulations in an indoor two-user 60 GHz environment if RF beam patterns of the users do not highly overlap in space.**

***Index Terms*—60 GHz radio, robust downlink beamforming, adaptive antenna arrays, SDMA and MU-MIMO.**

I. Introduction

THE increasing demands on bandwidths for personal wireless applications such as uncompressed multimedia streaming in indoor environments illustrated in Fig. 1 have driven the research and development for a new generation of broadband wireless personal and local area networks (WPAN/WLAN) [1]–[4]. The characteristics of broad and worldwide unlicensed bandwidth (BW) and high penetration losses at 60 GHz radio [5], [6] make it an ideal air interface for such indoor wireless applications. On one hand, emerging 60 GHz WPAN standards [1], [2] consider data transmission rates up to 5 $\sim$ 7 Gbit/s to provide wireless substitutes of universal serial bus (USB) 3.0 or high definition media interface (HDMI) 1.4. On the other hand, IEEE 802.11ad [3] and WiGig [4] are working on 60 GHz enhancement over the legacy IEEE 802.11 standard.

Despite the wider available BW, to provide high received signal qualities for 60 GHz radio, it seems necessary to offer high directivity in antenna patterns due to the strong oxygen absorption at 60 GHz [5], [6] and the smaller allowable transmit power over a 50 times wider BW than the legacy IEEE802.11 [7]. Thanks to the millimeter wavelength of 60 GHz radio, it appears feasible to use Phased Arrays of tiny patch Antennas (PAA) to provide the directivity with

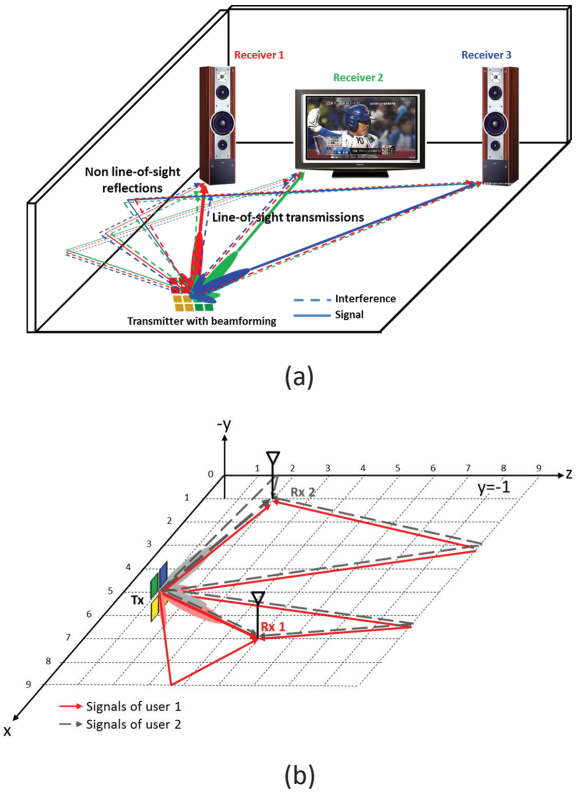

Fig. 1. An illustration of indoor 60 GHz applications for uncompressed wireless multimedia streaming. Subplot (b) shows a simulated 60 GHz indoor multipath channel of SDMA using phased antenna arrays.

Manuscript received November 8, 2012; revised April 1, 2013; accepted June 6, 2013. The associate editor coordinating the review of this paper and approving it for publication was M. McKay.

This research has been funded in part by the NCTU MTK Research Center, Taiwan, and in part by the National Science Council, Taiwan, under Grant NSC 98-2221-E-009-055. This paper has been presented in part at the IEEE Personal, Indoor and Mobile Radio Communications (PIMRC), 2009, Tokyo, Japan, and in part at the IEEE PIMRC, 2010, Istanbul, Turkey.

S.-H. Wu and L.-K. Chiu are with the Institute of Communications Engineering, Department of Electrical and Computer Engineering, National Chiao Tung University, Hsinchu, Taiwan, R.O.C. (e-mail: sauhsuan@cm.nctu.edu.tw, sazabi.cm96g@nctu.edu.tw).

K.-Y. Lin is with the Ministry of Justice, Investigation Bureau, Taiwan, R.O.C. (e-mail: linkoyen@gmail.com).

T.-H. Chang is with the Department of Electronic and Computer Engineering, National Taiwan University of Science and Technology, Taipei, Taiwan, R.O.C. (e-mail: tsunghui.chang@ieee.org).

Digital Object Identifier 10.1109/TWC.2013.072313.121749

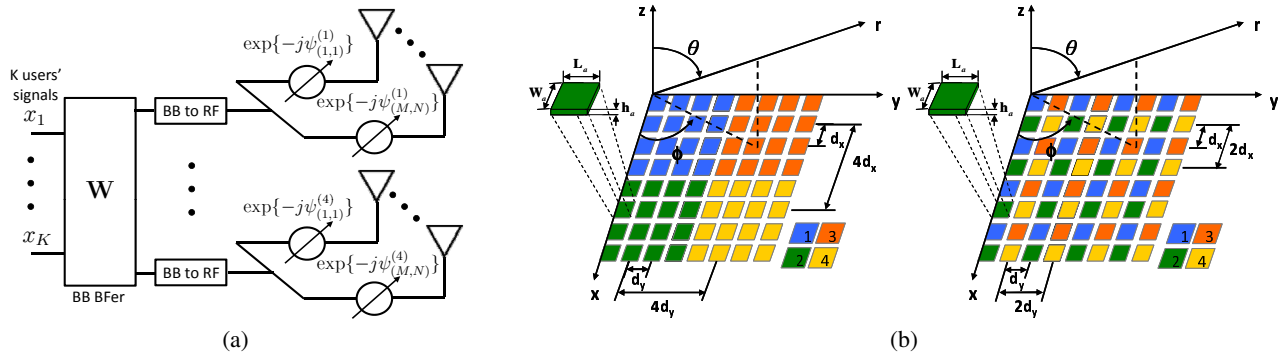

Fig. 2. Hybrid beamforming architecture for SDMA with phased antenna arrays (PAA). Subplot (b) presents two types of partitions for an 8×8 PAA. The left one stands for the type I partition, and the right one for the type II partition. Antennas in the same color are driven by the same BB-to-RF module.

beamforming (BF) [8], [9]. In view of the importance of directional transmission, BF with PAA has attracted recent research attentions both in academia and in 60 GHz WPAN/WLAN standards [8]–[10].

In typical BF with PAA at 60 GHz, each element patch antenna is equipped with a phase shifter to adjust the signal phase radiating through it such that the collective radio frequency (RF) signals form a constructive interference in the intended direction. The entire PAA is driven by a single baseband (BB) processing module only, *e.g.* [8]–[10]. This kind of PAA architectures is practical for implementations, however, restricts BB algorithms from exploiting the spatial diversity and multiplexing (DnM) advantages available from the multiple antennas of PAA. Recent studies in [11]–[17] and the standards body WirelessHD [2] start to reconsider hybrid PAA architectures for indoor 60 GHz radio attempting to simultaneously exploit the directivity with RF BF and the DnM advantages using multiple BB processing modules. A BB module considered in these hybrid architectures may drive only part of the antennas in PAA, as shown in Fig. 2 [11]–[16], or all of them [17], [18]. This type of architectures is not only for cost-effectiveness as opposed to using individual modules for every single antenna. But, more importantly, it is because the DnM advantage may not scale proportionally with the number of BB modules, due to the strong spatial correlations within the multi-millimeter antenna distances in PAA [5], [16], [19].

Even though providing high directivity in line-of-sight transmission (LOS) plays a crucial role for 60 GHz radio [20], and existing direction estimation mechanisms have been provided in IEEE standards [1], [3] or literatures [21], [22], for multimedia applications illustrated in Fig. 1, the transmitter still needs to frequently switch its beam towards receivers in different directions, which makes it challenging to provide realtime data streaming to the different receivers in a time-division multiple access (TDMA) manner [23]. Motivated by these practical limitations and the potential DnM advantages available in PAA, we consider hybrid architectures in Fig. 2 to support multi-user (MU) downlink (DL) transmissions in 60 GHz radio, making use of the concept of spatial-division multiple-access (SDMA) and MU multiple-input multiple output (MU-MIMO) systems. A similar architecture was studied in [15] for direction estimation of received signals.

Although, there have been rich results in both the SDMA and MIMO technologies, the related results for 60 GHz WPAN/WLAN are rather limited [11]–[18], [23]. Part of the reasons lies in the need to explore the unique features of indoor 60 GHz radio from that of the typical MIMO systems in lower frequencies. For single-user (SU) systems, [16] studies the MIMO capacity of a simpler architecture that uses a BB module for each separated PAA, and [17], [18], on the other hand, consider a more complicated mixed analog/digital BF architecture for joint transmit and receive signal processing in an indoor non-LOS (NLOS) 60 GHz environment.

For MU systems, [12] studies the capacities of indoor 60 GHz SDMA channels of using multiple linear or circular phased arrays, and [23] proposes a medium access control (MAC) protocol for SDMA in 60 GHz WLAN. Generalizing the non-robust hybrid beamforming (HBF) architecture in our previous works for SDMA in flat fading channels [13], [14], we develop herein robust HBF criteria and algorithms to combat the multiple access inference (MAI), inter-symbol interference (ISI), and model uncertainties from the phase shifter errors of PAA in MU DL SDMA. The main idea is to jointly exploit the indoor 60 GHz channel characteristics, and the spatial diversities offered by the high-directivity RF beam patterns and the MU-MIMO BB processing. The contributions and important features of our proposed criteria are introduced below. In contrast, a HBF architecture was studied in [24] for SU detection in typical flat-faded MU-MIMO channels.

Considering the feasibility and implementation cost of HBF for the multi-GHz BW of 60 GHz WPAN/WLAN, we study time-domain DL BF methods that only require the feedback of radio signal strength indicator (RSSI) and the prior knowledge on the intended transmit directions. The RSSI is typically used for establishing wireless transmission links, and the transmit direction can be readily obtained with the methods proposed in [21], [22] for 60 GHz standards [1], [3]. The proposed HBF architecture can thus be applied to systems that employ single-carrier frequency domain equalization (SC-FDE) [25], [26] or orthogonal frequency-domain multiplexing (OFDM). Both technologies have been adopted in major 60 GHz WPAN/WLAN standards [1]–[4].

To control the reception quality of SDMA in indoor 60 GHz multipath channels [20] without the full channel state information (CSI) feedbacks, we make use of the directivity provided by PAA and the large Rician K-factors of 60 GHz channels in LOS transmissions [20] through which high-

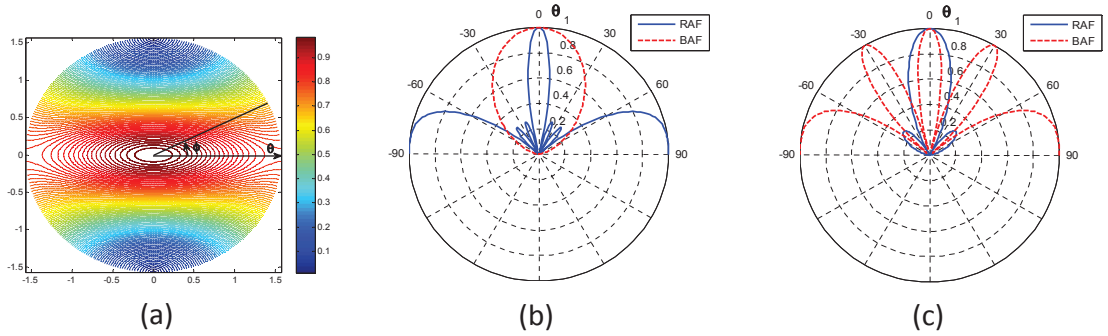

Fig. 3. The normalized contour plot of $|E(\phi,\theta)|$, and the normalized RAFs and BAFs of the type I and II partitions in Fig. 2. Subplots (b) and (c) show for the type I and II, respectively, the RAFs and BAFs.

definition multimedia streaming are typically applied [1]–[4]. These two features, on one hand, make it more effective to combat MAI and ISI with time-domain HBF, on the other hand, make signal qualities more sensitive to the phase shifter errors since both array gains and directivity degrade significantly in case of phase misalignments in RF signals [27]. To resolve the dilemma, we propose three types of formulations for beamformers (BFers) syntheses with increased levels of robustness to maintain the target signal to interference-plus-noise ratio (SINR) under MAI, ISI and phase shifter errors. We summarize our main contributions as below:

- A cost-effective hybrid architecture of PAA to support MU DL BF in indoor 60 GHz channels.
- A robust formulation that requires RSSIs and transmission directions to combat MAI and ISI.
- An uncertainty model that quantifies array gain degradations induced by phase errors in HBF.
- An extended robust formulation based on the S-Procedure [28] to combat phase uncertainties.
- An extended nonlinear robust formulation that results in semi closed-form expressions of BFers.

The HBF architecture will be described in Section II, and the unique features of the three robust formulations will be specified in Section III, IV and V respectively. Simulations in an indoor environment as illustrated in Fig. 1 show that phase uncertainties have a dominant impact on system performance. The robustness aimed to combat the uncertainties helps mitigate MAI as well. More simulation studies and discussions will be provided in Section VI and VII.

II. Hybrid Beamforming Architecture for SDMA with PAA

We start by introducing the configurations of PAA for HBF. Each patch antenna of a PAA is equipped with a phase shifter to maneuver the phase of the RF signal radiating through it. And a PAA is partitioned into blocks, each of which is driven by a BB processing module as illustrated in Fig. 2. This type of hybrid architectures has the flexibility to provide high directivity in its RF beam pattern when applied to a SU system, or to jointly exploit the directivity and spatial diversity in a MU DL SDMA system. We herein study the latter one. Other applications of this type of architectures can be found in [11], [13]–[15] as well. The composite beam pattern of this hybrid type of RF and BB BF method depends on the radiation pattern of the patch antenna, the partition of the PAA, the setting of the phase shifters and the BB BF weights. To compare the HBF performance of different partitions, two presentative types of partitions are considered in this paper, which can support DL SDMA for up to four users as illustrated in Fig. 2(b).

A. Patch Antenna Pattern and Radio Frequency Array Factor

We first briefly review the patch antenna pattern and the RF array factor (RAF) of the two PAA partitions of Fig 2(b), which will be used throughout the paper. Define a direction pair (ϕ,θ) where ϕ is the azimuth angle and θ is the elevation angle in the coordinate system of Figs. 1(b) and 2(b). The far-zone electric field of a patch antenna in the direction of (ϕ,θ) follows

$$E(\phi,\theta) = E_\theta \overrightarrow{e_\theta} + E_\phi \overrightarrow{e_\phi} + E_r \overrightarrow{e_r} \tag{1}$$

where $E_r \cong 0$ along the radial direction, $\overrightarrow{e_r}$, as we assume $r \gg \frac{2L_aW_a}{\lambda}$ (see [29] for the far field definition), and the other two components in $\overrightarrow{e_\theta}$ and $\overrightarrow{e_\phi}$ are given, respectively, by

$$E_\theta = E_0' \cos\phi \cos X \left(\frac{\sin Y}{Y}\right)\left(\frac{\sin Z}{Z}\right) \tag{2}$$

$$E_\phi = E_0' \cos\theta \sin\phi \cos X \left(\frac{\sin Y}{Y}\right)\left(\frac{\sin Z}{Z}\right) \tag{3}$$

with $E_0' \triangleq j\frac{2h_aW_aE_0\exp\{-j\frac{2\pi}{\lambda}r\}}{\lambda r}$, $X \triangleq \frac{\pi L_a}{\lambda}\sin\theta\cos\phi$, $Y \triangleq \frac{\pi W_a}{\lambda}\sin\theta\sin\phi$ and $Z \triangleq \frac{\pi h_a}{\lambda}\cos\theta$. The parameter λ is the wavelength and E_0 is a constant related to antenna design [29]. For other parameters in the expressions, their physical meanings are illustrated in Fig. 2. The contour plot of the normalized $|E(\phi,\theta)|$ is shown in Fig. 3(a) in a cylindrical coordinate whose angular coordinate corresponds to ϕ, and radial coordinate corresponds to θ in the coordinate of Fig. 2(b). The antenna pattern is generated with $L_a = W_a = 1.3$ mm and $h_a = 0.127$ mm in [30].

Suppose that patch antennas in PAA are all identical and that the coupling effects among the antennas can be neglected. By the antenna array theory, the RAF of a block i is given by (4) where $\Psi_x(\phi,\theta) \triangleq \frac{2\pi}{\lambda}d_x\cos\phi\sin\theta$ and $\Psi_y(\phi,\theta) \triangleq \frac{2\pi}{\lambda}d_y\sin\phi\sin\theta$. The letters N and M represent, respectively, the numbers of antennas in the x and y directions of a block.

$$A^{(i)}(\phi,\theta) \triangleq \frac{1}{\sqrt{MN}} \sum_{n=1}^{N} \sum_{m=1}^{M} \exp\{j(n-1)a_x\Psi_x(\phi,\theta) + j(m-1)a_y\Psi_y(\phi,\theta) - j\psi_{(n,m)}^{(i)}\} \quad (4)$$

A patch antenna indexed by (n,m) stands for an antenna located at the n-th position, $n \in \{1,\ldots,N\} \triangleq \mathcal{I}_N$ [1], in the x direction and the m-th position, $m \in \mathcal{I}_M$, in the y direction of a block. The variable $\psi_{(n,m)}^{(i)}$, thus, represents the phase offset introduced by the phase shifter of antenna (n,m) of block i. For the PAAs in Fig. 2(b), we have $M = N = 4$, and $i \in \mathcal{I}_4$. The indices, i, for each type of partition are shown in the lower right corners of their corresponding plots in Fig. 2(b).

The values of $(n-1)a_xd_x$ and $(m-1)a_yd_y$ are the distances in the x and y directions, respectively, between antennas (n,m) and $(1,1)$ of the same block. The values of (a_x,a_y) for adjacent patch antennas depend on the partition. For the type I partition, $(a_x,a_y) = (1,1)$, and for the type II, $(a_x,a_y) = (2,2)$. Given the target direction $\left(\varphi^{(i)},\vartheta^{(i)}\right)$ for block i, ideally, we can set

$$\psi_{(n,m)}^{(i)} = (n-1)a_x\Psi_x\left(\varphi^{(i)},\vartheta^{(i)}\right) + (m-1)a_y\Psi_y\left(\varphi^{(i)},\vartheta^{(i)}\right) \quad (5)$$

to maximize $A^{(i)}(\phi,\theta)$ in the direction of $\left(\varphi^{(i)},\vartheta^{(i)}\right)$, which allows us to steer the main beam of (4) of a block to point to different directions.

B. Hybrid Beamforming Pattern

In indoor 60 GHz radio, propagations suffer from additional 20 dB free space losses compared to the legacy 802.11 WLAN [6], [7]. But in a relatively shorter operating range that requires 10 dB less transmission power [7], the maximum array gain, $|A^{(i)}(\phi,\theta)| \doteq 12$ dB, of a 4×4 block can help make up the extra 10dB power requirement. Despite the array gain, users' signals may severely affect each other by the side lobes and grating lobes of their RAFs in (4). The grating lobes depend on (a_x,a_y) and the antenna spacing $(d_x,\ d_y)$. In this paper, we set $d_x = d_y = \frac{\lambda}{2} = 2.5$ mm. Therefore, the grating lobes are affected by (a_x,a_y) only. The normalized RAFs, $\frac{|A^{(i)}(0,\theta)|}{\max_\theta |A^{(i)}(0,\theta)|}$, of a block of the type I and II partitions are shown in Figs. 3 (b) and (c), respectively, when $\vartheta^{(i)} = 0$.

In addition to MAI from side lobes or grating lobes, signals of users may also interfere with each other through NLOS reflections in indoor 60 GHz channels [31], [32]. To maintain the SINR for each user in such MAI and ISI channels, users' symbols are precoded in BB before transmission.

Suppose that $\mathbf{w}_p^T \triangleq \left[w_p^{(1)}\ \ldots\ w_p^{(4)}\right]$ is the BB BF weight vector used to linearly precode the modulated symbols of user p. The HBF pattern for user p is thus expressed as

$$H_p(\phi,\theta) \triangleq E(\phi,\theta)\sum_{i=1}^{4} A^{(i)}(\phi,\theta)w_p^{(i)} \exp\left\{j(b_x^{(i)}\Psi_x(\phi,\theta) + b_y^{(i)}\Psi_y(\phi,\theta))\right\}. \quad (6)$$

The values of $b_x^{(i)}d_x$ and $b_y^{(i)}d_y$ are the distances in the x and y directions, respectively, between block i and block 1 of a type of partitions in Fig. 2. For instance, we have $b_x^{(4)} = 4$ and $b_y^{(4)} = 4$ for the type I partition, and $b_x^{(4)} = 1$ and $b_y^{(4)} = 1$ for the type II. Due to the BF weight $\mathbf{w}_p$, the composite HBF patterns are affected by both the RAF and the BB *array factor* (BAF) of $\mathbf{w}_p$. The normalized BAFs of the type I and II partitions are shown in Fig. 3 as well, generated with $|H_p(\phi,\theta)|$ by setting $E(\phi,\theta) = 1$, $A^{(i)}(\phi,\theta) = 1$, and $w_p^{(i)} \triangleq \frac{1}{\sqrt{4}} \exp\left\{-j(b_x^{(i)}\Psi_x(\varphi^{(i)},\vartheta^{(i)}) + b_y^{(i)}\Psi_y(\varphi^{(i)},\vartheta^{(i)}))\right\}$, $\forall i \in \mathcal{I}_4$, to compensate the effects of block distances in the target direction of $\vartheta^{(i)} = 0$.

Results in Fig. 3 show that the double inter-antenna spacing, $(a_x,a_y) = (2,2)$, in a block of the type II partition results in grating lobes in its RAF. On the other hand, the quadruple inter-block distance of the type I partition will yield grating lobes in its BAF. The PAA partition, thus, has direct impact on the HBF pattern. And equations (4) and (6) suggest that one should jointly design the BB BFers $\mathbf{w}_p$ and the values of $\psi_{(n,m)}^{(i)}$ for all patch antennas. In practice, the phase shifters can often be set only to a limited number of predefined angles, in particular, at such a high frequency of 60 GHz [9], [33]. Suppose that the number of adjustable angles is N_p. Ideally we will have a discrete set $\mathbf{\Xi} \triangleq \left\{2\pi(\ell-1)/N_p \,\middle|\, \ell \in \mathcal{I}_{N_p}\right\}$ for $\psi_{(n,m)}^{(i)}$. Under the constraint of $\psi_{(n,m)}^{(i)} \in \mathbf{\Xi}$, $\mathbf{w}_p$ should be evaluated for N_p^{4MN} possible combinations of $\psi_{(n,m)}^{(i)}$. Taking for instance the designs of [8], [10], a reasonable value of N_p is 8, making $N_p^{4MN} = 2^{192}$ in our system setting. This leaves us no choice but to consider a low-complexity HBF design.

Intuitively, one would associate a block of the PAA to an individual user p, and simply maximizes its RAF in the LOS direction $(\phi_{p,0},\theta_{p,0})$ of its associated user with (5). Though straightforward, this simple approach allows us to separate the design of $\mathbf{w}_p$ from that of $\psi_{(n,m)}^{(i)}$. And the array gain of RAF can provide each user a certain degree of SINR in advance if users' signals have proper separations in space. Moreover, the high directivity of the RAF of a large block can help pre-confine the interference of a user's signal in MAI and ISI channels as well, due to the high reflection and path losses of the 60 GHz radio in indoor environments. Nevertheless, under the constraint of $\psi_{(n,m)}^{(i)} \in \mathbf{\Xi}$, this still requires to determine the set $\mathbf{\Psi}^{(i)}$ of $\psi_{(n,m)}^{(i)}$, $\forall i \in \mathcal{I}_4$, with

$$\mathbf{\Psi}^{(i)} \triangleq \{\psi_{(n,m)}^{(i)} \Big|\ \max|A^{(i)}(\phi_{p,0},\theta_{p,0})|,\ \psi_{(n,m)}^{(i)} \in \mathbf{\Xi}, \ n = 1,\ldots,N,\ m = 1,\ldots,M\}. \quad (7)$$

The complexity of this scheme is still $4(N_p^{MN}) = 2^{50}$ in our system setting. Considering the feasibility in practice, a heuristic method that does not necessarily maximize the RAF is needed.

Observe from (4) that the RAF is deterministic as long as $\psi_{(n,m)}^{(i)}$ are set exactly to values in $\mathbf{\Xi}$ even if the RAF is not maximized with (7). The degradation in the RAF can be compensated with $\mathbf{w}_p$ if N_p of $\mathbf{\Xi}$ is not too small, and

[1] We use $\mathcal{I}_n$ in the sequel to represent an index set of $\{1,2,\ldots,n\}$.

the errors coupled on $\psi^{(i)}_{(n,m)}$ are negligible. The challenges to HBF designs are, therefore, more from the uncertainty in each discrete angle of each phase shifter than from the number of discrete angles, N_p. This motives us to use a simple quantizer

$$\arg\min_{\psi\in\mathbf{\Xi}} |\psi - \psi^{(i)}_{(n,m)} \mod 2\pi|^2 \tag{8}$$

to set phase shifters to values nearest to $\psi^{(i)}_{(n,m)}$ of (5) in $\mathbf{\Xi}$, and design robust BFers $\mathbf{w}_p$ to maintain the SINR under the phase shifter errors. Our simulation results in Section VI will show that the performance of using (8) with $N_p = 8$ is fairly close to, and in some cases even better than, that of setting the exact $\psi^{(i)}_{(n,m)}$ of (5) for phase shifters. This validates our design approach, yet, also implies that a full HBF design can be non-trivial, even though it remains challenging to verify how close an approximate design with (8) can approach the optimal HBF one. In the sequel, we focus on developing BF schemes to construct $\mathbf{w}_p$ under various design constraints in MU DL SDMA. The performance of the two types of partitions will be studied by simulations in Section VI from the perspectives of BFers' power consumptions and SINR satisfaction ratios.

III. Baseband Design of HBF for Multiuser Downlink SDMA

According to (6), the signal received in the direction $(\phi_{p,\ell}, \theta_{p,\ell})$ of the ℓ-th path to user p is

$$\sqrt{\mathcal{L}_{p,\ell}} h_{p,\ell} E_{p,\ell} [A^{(1)}_{p,\ell} \exp\{j(b^{(1)}_x \Psi_{x,p,\ell} + b^{(1)}_y \Psi_{y,p,\ell})\}, \ldots, A^{(4)}_{p,\ell} \exp\{j(b^{(4)}_x \Psi_{x,p,\ell} + b^{(4)}_y \Psi_{y,p,\ell})\}] \mathbf{W}\mathbf{x} \tag{9}$$

where $\mathbf{W} \triangleq [\mathbf{w}_1 \ldots \mathbf{w}_K]$ and $\mathbf{x} \triangleq [x_1, \ldots, x_K]^T$ with T standing for matrix transpose and $K \leq 4$ being the number of users. The power of users' signals, x_p, is normalized to $\mathbb{E}\{|x_p|^2\} = 1$, $\forall p \in \mathcal{I}_K$, with $\mathbb{E}\{\cdot\}$ standing for expectation. Let L_p be the number of channel paths to user p. By the method of (5) and (8), the RAF, $A^{(i)}_{p,\ell}$, of a block $i \in \mathcal{I}_4$ is the value of $A^{(i)}(\phi_{p,\ell}, \theta_{p,\ell})$ observed at $(\phi_{p,\ell}, \theta_{p,\ell})$, $\forall \ell \in \mathcal{I}_{L_p-1}$, when its target direction is set to the LOS direction, $(\phi_{p,0}, \theta_{p,0})$, of its associated user p. Following this notational convention, we also define $\mathcal{L}_{p,\ell}$ to be the power propagation loss along the direction of $(\phi_{p,\ell}, \theta_{p,\ell})$, and have $E_{p,\ell} \triangleq \frac{E(\phi_{p,\ell},\theta_{p,\ell})}{\oint\oint E(\phi,\theta) d\phi d\theta}$, $\Psi_{x,p,\ell} \triangleq \Psi_x(\phi_{p,\ell}, \theta_{p,\ell})$ and $\Psi_{y,p,\ell} \triangleq \Psi_y(\phi_{p,\ell}, \theta_{p,\ell})$. The time-domain NLOS channel coefficients, $h_{p,\ell}$, are independent and complex Gaussian distributed with zero-mean and $\mathbb{E}\{|h_{p,\ell}|^2\} = 1$, $\forall \ell \in \mathcal{I}_{L_p-1}$. For the LOS channels, however, $|h_{p,0}| = 1$ and $\measuredangle h_{p,0}$ are uniformly distributed in $[0, 2\pi)$ [3], [32].

The expression of (9) motivates us to define a steering vector for each direction $(\phi_{p,\ell}, \theta_{p,\ell})$ as

$$\mathbf{s}_{p,\ell} \triangleq \Big[\exp\{j(b^{(1)}_x \Psi_{x,p,\ell} + b^{(1)}_y \Psi_{y,p,\ell})\}, \ldots, \exp\{j(b^{(4)}_x \Psi_{x,p,\ell} + b^{(4)}_y \Psi_{y,p,\ell})\}\Big]^\dagger \tag{10}$$

to quantify the phase differences among antenna blocks, where $\dagger$ stands for conjugate transpose. Further, let $\mathbf{A}_{p,\ell} \triangleq \text{diag}\{[A^{(1)}_{p,\ell}, A^{(2)}_{p,\ell}, A^{(3)}_{p,\ell}, A^{(4)}_{p,\ell}]\}$ be a diagonal matrix. By (9) and (10), the average power received at user p from the signal component of user q can thus be expressed as

$$\sum_{\ell=0}^{L_p-1} \mathcal{L}_{p,\ell} |E_{p,\ell} \mathbf{s}^\dagger_{p,\ell} \mathbf{A}_{p,\ell} \mathbf{w}_q|^2 \triangleq \sum_{\ell=0}^{L_p-1} \mathcal{L}_{p,\ell} |\mathbf{g}^\dagger_{p,\ell} \mathbf{w}_q|^2, \ \forall p, q \in \mathcal{I}_K \tag{11}$$

with $\mathbf{g}_{p,\ell} \triangleq E^*_{p,\ell} \mathbf{A}^\dagger_{p,\ell} \mathbf{s}_{p,\ell}$ being viewed as the effective beam pattern along the ℓ-th path to user p.

Based on (11), the time-domain average SINR then follows

$$\text{SINR}_p \triangleq \frac{\sum_{\ell=0}^{L_p-1} \mathcal{L}_{p,\ell} |\mathbf{g}^\dagger_{p,\ell} \mathbf{w}_p|^2}{\sum_{q\neq p}^{K} \sum_{\ell=0}^{L_p-1} \mathcal{L}_{p,\ell} |\mathbf{g}^\dagger_{p,\ell} \mathbf{w}_q|^2 + \sigma_p^2} \tag{12}$$

where σ_p^2 is the noise variance at user p. In this paper, we use this average SINR as a performance metric to maintain the signal quality for each user in MU DL SDMA systems.

Define a quality constraint, γ_0, on the SINR_p. The optimization problem to minimize the transmission power subject to (*s.t.*) $\text{SINR}_p \geq \gamma_0$ is a typical quadratic constrained quadratic programming (QCQP) problem [28]. For clarity, we, instead, refer to this programming problem as an SINR constrained power minimization (SCPM) problem, and formulate it in our setting as

$$\begin{aligned} &\arg\min_{\{\mathbf{w}_p\}_{p=1}^K} \textstyle\sum_{p=1}^K \|\mathbf{w}_p\|^2 \\ s.t. \quad &\tfrac{1}{\gamma_0} \mathbf{w}^\dagger_p (\mathbf{Q}_p + \Delta\mathbf{Q}_p) \mathbf{w}_p \geq \\ &\qquad \sum_{q=1, q\neq p}^{K} \mathbf{w}^\dagger_q (\mathbf{Q}_p + \Delta\mathbf{Q}_p) \mathbf{w}_q + \sigma_p^2, \ \forall p \in \mathcal{I}_K \end{aligned} \tag{13}$$

where $\mathbf{Q}_p \triangleq \mathcal{L}_{p,0} \mathbf{g}_{p,0} \mathbf{g}^\dagger_{p,0}$ and $\Delta\mathbf{Q}_p \triangleq \sum_{\ell=1}^{L_p-1} \mathcal{L}_{p,\ell} \mathbf{g}_{p,\ell} \mathbf{g}^\dagger_{p,\ell}$. The total transmit power delivering to the PAA is equal to $\sum_{p=1}^K \|\mathbf{w}_p\|^2$ since $A^{(i)}_{p,\ell}$ and $E_{p,\ell}$ have been normalized in (4) and (9).

Given $\mathbf{Q}_p$ and $\Delta\mathbf{Q}_p$, the problem can be solved with the fixed-point method developed in [34], or be reformulated as a second-order cone programming problem, and solved using SeDuMi or CVX [35], [36]. In practice, however, the complexity to estimate the sum of $\mathbf{Q}_p$ and $\Delta\mathbf{Q}_p$ is typically high. A feasible way is to estimate it from the autocorrelation matrix of the frequency-domain channel responses. Specifically, let $[\mathbf{g}_{p,\ell}]_i$ be the i-th element of $\mathbf{g}_{p,\ell}$. The frequency-domain channel coefficient from an antenna block i to user p is given by $\mathcal{H}_{p,f_t,i} \triangleq \sum_{\ell=0}^{L_p-1} h_{p,\ell} \sqrt{\mathcal{L}_{p,\ell}} [\mathbf{g}_{p,\ell}]_i \exp\{-j\frac{2\pi f_t \ell}{N_F}\}$ where $f_t \in \{0, \ldots, N_F - 1\}$ with N_F being the number of subcarriers of OFDM. Define $\underline{\mathcal{H}}_{p,f_t} \triangleq [\mathcal{H}_{p,f_t,1}, \ldots, \mathcal{H}_{p,f_t,4}]^T$. Then it is straightforward to show that $\mathbb{E}\{\underline{\mathcal{H}}_{p,f_t} \underline{\mathcal{H}}^\dagger_{p,f_t}\} = \sum_{\ell=0}^{L_p-1} \mathcal{L}_{p,\ell} \mathbf{g}_{p,\ell} \mathbf{g}^\dagger_{p,\ell} = \mathbf{Q}_p + \Delta\mathbf{Q}_p \simeq \frac{1}{N_F} \sum_{f_t=0}^{N_F-1} \underline{\mathcal{H}}_{p,f_t} \underline{\mathcal{H}}^\dagger_{p,f_t}$. Based on this approximation, each user p can estimate and feed back its $\mathbf{Q}_p + \Delta\mathbf{Q}_p$ to the transmitter to solve (13). Apparently, the complexity and feedback overhead for this type of BF design is quite high. In the sequel, we consider an alternative design methodology that exploits the indoor 60 GHz channel characteristics to reduce the complexity and, in particular, the feedback overhead.

A. Robust BF Design to Combat MAI and ISI with Partial CSI at the Transmitter

When applying BF in 60 GHz radio, the received power is in general dominated by its LOS component. The reasons

TABLE I
THE VALUES OF κ_1 AND κ_2 GENERATED WITH THE TYPE II PARTITION IN FIG. 2.

	κ_1/κ_2	z_2 = 2	3	4	5	6	7	8	9
	0	21/20	21/25	20/48	27/63	53/33	100/24	133/9	146/66
	1	21/12	20/15	23/25	56/27	118/28	140/16	158/7	166/7
	2	21/23	20/42	54/71	130/70	152/50	161/22	120/9	76/9
	3	20/65	53/163	142/109	162/50	95/30	53/13	41/6	37/8
x_2	4	54/554	163/211	54/96	37/42	33/17	30/10	28/7	26/12
	5	21/279	21/66	21/35	21/23	20/20	21/21	21/30	21/36
	6	43/401	143/578	71/93	32/36	23/15	20/9	20/6	20/11
	7	25/54	45/126	158/96	141/140	114/33	71/18	45/8	31/7
	8	22/17	30/28	46/31	129/34	158/36	144/47	124/8	97/11
	9	22/29	25/32	33/56	46/33	100/26	163/19	163/9	139/131

are three-fold: First, the array gain in the LOS direction is typically much higher than those in the NLOS directions if the beam pattern of a RAF is properly steered towards its intended receiver. Second, the power losses from NLOS reflections are around 10 dB for the first reflections, and are 6 dB more for the second reflections in indoor 60 GHz channels [32]. Third, the longer traveling distances of NLOS reflections also contribute extra losses, in particular, under the strong oxygen absorption effect at 60 GHz [6], [20]. Due to the dominance of LOS components, the Rician K-factors [37] of indoor 60 GHz channels are expected to be high.

Define the Rician K-factor, also acknowledged as the K-factor, for the channel of user p by

$$\kappa_p \triangleq \frac{\mathcal{L}_{p,0}\|\mathbf{g}_{p,0}\|^2}{\sum_{\ell=1}^{L_p-1}\mathcal{L}_{p,\ell}\|\mathbf{g}_{p,\ell}\|^2} = \frac{\mathcal{L}_{p,0}|E_{p,0}|^2\sum_{i=1}^{4}|A_{p,0}^{(i)}|^2}{\sum_{\ell=1}^{L_p-1}\mathcal{L}_{p,\ell}|E_{p,\ell}|^2\sum_{i=1}^{4}|A_{p,\ell}^{(i)}|^2}. \quad (14)$$

The K-factors of users 1 and 2 of a two-user system are shown in Table I, which are simulated based on the channel model of [32], [38] for a $9\times5\times9$ m^3 conference room illustrated in Fig. 1(b). In simulations, the transmitter and the receivers are all placed on the plane of $y=-1$ in the Cartesian coordinate of Fig. 1(b). Therefore, the location of the transmitter is denoted by (x_T, z_T), for simplicity, and the locations of a receiving user, p, is denoted by (x_p, z_p), $\forall p \in \mathcal{I}_K$.

The values of an entry (x_2, z_2) are the K-factors κ_1 and κ_2 when $(x_T, z_T) = (5, 1)$, $(x_1, z_1) = (7, 5)$, and user 2 is at the location (x_2, z_2) in Fig. 1(b). The K-factors of each location are evaluated averaging over 1000 simulated channels when the RAFs are generated according to the type II partition in Fig. 2, with $A_{p,\ell}^{(1)}$ and $A_{p,\ell}^{(4)}$ steered towards user 1 and the other two steered towards user 2. Although the K-factors vary with (x_2, z_2), their values are greater than 10 in 66 out of 80 locations, which justify our argument that the received power is in general dominated by its LOS component. For more details about channel simulations, please refer to Section VI.

Suppose that $\kappa_p \gg 1$, then $\mathcal{L}_{p,0}\|\mathbf{g}_{p,0}\|^2 \simeq \sum_{\ell=0}^{L_p-1}\mathcal{L}_{p,\ell}\|\mathbf{g}_{p,\ell}\|^2$, which is equal to the RSSI value. The RSSI feedback is often required by a transmitter to establish a transmission rate to its intended receiver. Given users' directions $(\phi_{p,0}, \theta_{p,0})$, and, hence, $\mathbf{g}_{p,0}$, the transmitter thus obtains the approximation of $\mathcal{L}_{p,0}$ from the RSSI feedback, which yields $\mathbf{Q}_p \triangleq \mathcal{L}_{p,0}\mathbf{g}_{p,0}\mathbf{g}_{p,0}^\dagger$. The uncertainty in the estimate of $\mathbf{Q}_p$ can be incorporated into $\Delta\mathbf{Q}_p$ that characterize the NLOS ISI.

Although $\Delta\mathbf{Q}_p$ is not available to the transmitter, by the definition of $\Delta\mathbf{Q}_p$, we have $\|\Delta\mathbf{Q}_p\|_{\mathcal{F}} \le \sum_{\ell=1}^{L_p-1}\|\mathcal{L}_{p,\ell}\mathbf{g}_{p,\ell}\mathbf{g}_{p,\ell}^\dagger\|_{\mathcal{F}}$, according to the triangle inequality. Set a lower bound for κ_p, and, hence, an upper bound, $\mathcal{K}_p$, on $\frac{1}{\kappa_p}\mathcal{L}_{p,0}\|\mathbf{g}_{p,0}\|^2$. By (14), we may reformulate the SCPM problem of (13) to account for all $\Delta\mathbf{Q}_p$ whose $\|\Delta\mathbf{Q}_p\|_{\mathcal{F}} \le \frac{1}{\kappa_p}\mathcal{L}_{p,0}\|\mathbf{g}_{p,0}\|^2 \le \mathcal{K}_p$ [39]–[41].[2] Specifically, we have

$$\begin{aligned} &\arg\min_{\{\mathbf{w}_p\}_{p=1}^K} \textstyle\sum_{p=1}^K \|\mathbf{w}_p\|^2 \\ s.t.\quad &\arg\min_{\|\Delta\mathbf{Q}_p\|_{\mathcal{F}}\le\mathcal{K}_p} \frac{\mathbf{w}_p^\dagger(\mathbf{Q}_p+\Delta\mathbf{Q}_p)\mathbf{w}_p}{\sum_{q=1,q\ne p}^K \mathbf{w}_q^\dagger(\mathbf{Q}_p+\Delta\mathbf{Q}_p)\mathbf{w}_q+\sigma_p^2} \ge \gamma_0, \\ &\forall p \in \mathcal{I}_K. \end{aligned} \quad (15)$$

Let $\mathbb{A}_p \triangleq \gamma_0\sum_{q=1,q\ne p}^K \mathbb{W}_q - \mathbb{W}_p$ with $\mathbb{W}_p \triangleq \mathbf{w}_p\mathbf{w}_p^\dagger$, $\forall p \in \mathcal{I}_K$. If we relax the rank-one constraint of rank$\{\mathbb{W}_p\} = 1$, the problem can be transformed with the method of [40] into

$$\begin{aligned} &\arg\min_{\{\mathbb{W}_p,\mathbb{B}_p\}_{p=1}^K} \textstyle\sum_{p=1}^K \mathrm{Tr}\{\mathbb{W}_p\} \\ s.t.\quad &\mathcal{K}_p\|\mathbb{A}_p+\mathbb{B}_p\|_{\mathcal{F}} + \mathrm{Tr}\{\mathbf{Q}_p(\mathbb{A}_p+\mathbb{B}_p)\} + \gamma_0\sigma_p^2 \le 0, \\ &\mathbb{B}_p \succeq \mathbf{0},\ \forall p \in \mathcal{I}_K \end{aligned} \quad (16)$$

where $\succeq \mathbf{0}$ stands for positive semidefinite (*p.s.d.*), and $\mathrm{Tr}\{\cdot\}$ stands for the trace of its argument.

This is a semidefinite programming (SDP) problem whose solutions were shown by large simulations in [40] to satisfy rank$\{\mathbb{W}_p\} = 1$. For succinctness, this criterion of (16) is denoted by SDP-R-SCPM to signify the SDP method in solving the robust SCPM (R-SCPM) problem of (15). We note that a matrix $\mathbb{B}_p$ is introduced in (16). And it also requires some knowledge on $\mathcal{K}_p$, namely, the lower bound of κ_p (14). The values of κ_p reflect the degree of ISI and vary with locations as shown in Table I. A smaller lower bound for κ_p gives a higher chance to satisfy the SINR constrain in more locations, but also entails more power. A reasonable value should be set based on observations, experiments and performance requirements. A similar concept and practice has long been adopted in setting the length of the cyclic prefix for OFDM or SC-FDE.

IV. ROBUST BF DESIGN FOR PAA WITH IMPERFECT PHASE SHIFTERS

Although the HBF scheme of (6), (8) and (16) allows us to maintain the SINR under MAI with a feasible complexity

[2]The values of $\mathcal{K}_p$ are set equal to $\frac{1}{\kappa}\mathcal{L}_{p,0}\|\mathbf{g}_{p,0}\|^2$ in simulations, with κ being the lower bound for κ_p, $\forall p \in \mathcal{I}_K$.

in MU DL SDMA, the performance of the HBF scheme is closely related to $|A_{p,0}^{(i)}|^2$, $\forall p \in \mathcal{I}_K$, whose values are determined by $\psi_{(n,m)}^{(i)}$ of the phase shifters, $\forall n \in \mathcal{I}_N$, $m \in \mathcal{I}_M$ and $i \in \mathcal{I}_4$. Despite that $\psi_{(n,m)}^{(i)}$ are quantized and set to discrete values by (8), whose true values are subject to variations from manufacturing, in particular at such a high frequency of 60 GHz [9], [33]. The foci of RAFs will thus become blurred since the phase errors vary for different patch antennas [9], [33]. As a result, the RAFs $A_i(\phi,\theta)$ for different blocks will not be the same even if setting $\psi_{(n,m)}^{(1)} = \psi_{(n,m)}^{(2)} \cdots = \psi_{(n,m)}^{(4)}$, $\forall n \in \mathcal{I}_N$ and $m \in \mathcal{I}_M$. In a MU SDMA system discussed herein, these uncertainties in the RAFs make it even more difficult to maintain the SINR for all users in the system, motivating us to combat the phase uncertainties with robust BF designs.

A. Effects of Phase Uncertainty in Phase Shifters

Denote the phase errors in $\psi_{(n,m)}^{(i)}$ by $\delta\psi_{(n,m)}^{(i)}$. The RAFs under the influences of $\delta\psi_{(n,m)}^{(i)}$ become

$$\widetilde{A}^{(i)}(\phi,\theta) = \frac{1}{\sqrt{MN}} \sum_{n=1}^{N}\sum_{m=1}^{M} \wp_{(n,m)}^{(i)}(\phi,\theta) \exp\left\{ j\delta\psi_{(n,m)}^{(i)} \right\} \tag{17}$$

with $\wp_{(n,m)}^{(i)}(\phi,\theta) \triangleq \exp\{j[(n-1)a_x\Psi_x(\phi,\theta) + (m-1)a_y\Psi_y(\phi,\theta)] - j\psi_{(n,m)}^{(i)}\}$. Since the phase errors are bounded and usually have $\max\{|\delta\psi_{(n,m)}^{(i)}|\} \leq 5^\circ$ and $\sqrt{E\{|\delta\psi_{(n,m)}^{(i)}|^2\}} \approx 2^\circ$ for PAAs designed for millimeter wave (mmWave) radio [9], [33], we thus define $|\delta\psi_{(n,m)}^{(i)}| \leq \varepsilon$. Given that ε is small, we have $\exp\{j\delta\psi_{(n,m)}^{(i)}\} \simeq 1 + j\delta\psi_{(n,m)}^{(i)}$. The RAF can thus be approximated as

$$\widetilde{A}^{(i)}(\phi,\theta) \simeq A^{(i)}(\phi,\theta) + \left(\underline{\wp}^{(i)}(\phi,\theta)\right)^{\dagger} \boldsymbol{\Delta}^{(i)} \tag{18}$$

with $\underline{\wp}^{(i)}(\phi,\theta) \triangleq \frac{j}{\sqrt{MN}}[\wp_{(1,1)}^{(i)}(\phi,\theta) \ \cdots \ \wp_{(1,M)}^{(i)}(\phi,\theta), \ \cdots, \ \wp_{(N,1)}^{(i)}(\phi,\theta) \ \cdots \ \wp_{(N,M)}^{(i)}(\phi,\theta)]^{\dagger}$ and the uncertainty vector defined as $\boldsymbol{\Delta}^{(i)} \triangleq [\delta\psi_{(1,1)}^{(i)} \cdots \ \delta\psi_{(1,M)}^{(i)}, \cdots, \delta\psi_{(N,1)}^{(i)} \ \cdots \ \delta\psi_{(N,M)}^{(i)}]^T$.

Due to the uncertainty term $\left(\underline{\wp}^{(i)}(\phi,\theta)\right)^{\dagger}\boldsymbol{\Delta}^{(i)}$ in (18), the HBF pattern of (6) should be modified accordingly to reflect the influences of phase errors. Denote $\widetilde{A}^{(i)}(\phi_{p,\ell},\theta_{p,\ell})$ by $\widetilde{A}_{p,\ell}^{(i)}$, for simplicity, which is associated with the ℓ-th incoming path to user p. Similarly, we also denote the corresponding $\underline{\wp}^{(i)}(\phi_{p,\ell},\theta_{p,\ell})$ by $\underline{\wp}_{p,\ell}^{(i)}$. Based on the result of (18), the HBF pattern becomes

$$\begin{aligned} \widetilde{H}_q(\phi_{p,\ell},\theta_{p,\ell}) &= E_{p,\ell}\mathbf{s}_{p,\ell}^{\dagger}\widetilde{\mathbf{A}}_{p,\ell}\mathbf{w}_q \\ &\simeq E_{p,\ell}\mathbf{s}_{p,\ell}^{\dagger}(\mathbf{A}_{p,\ell} + \Delta\mathbf{A}_{p,\ell})\mathbf{w}_q \\ &\triangleq \widetilde{\mathbf{g}}_{p,\ell}^{\dagger}\mathbf{w}_q = \mathbf{g}_{p,\ell}^{\dagger}\mathbf{w}_q + \Delta\mathbf{g}_{p,\ell}^{\dagger}\mathbf{w}_q \end{aligned} \tag{19}$$

where $\Delta\mathbf{A}_{p,\ell} \triangleq \text{diag}\left\{\left[\left(\underline{\wp}_{p,\ell}^{(1)}\right)^{\dagger}\boldsymbol{\Delta}^{(1)} \ldots \left(\underline{\wp}_{p,\ell}^{(4)}\right)^{\dagger}\boldsymbol{\Delta}^{(4)}\right]\right\}$, $\widetilde{\mathbf{A}}_{p,\ell} \triangleq \text{diag}\left\{\left[\widetilde{A}_{p,\ell}^{(1)} \ldots \widetilde{A}_{p,\ell}^{(4)}\right]\right\}$ and $\Delta\mathbf{g}_{p,\ell} \triangleq E_{p,\ell}\mathbf{s}_{p,\ell}^{\dagger}\Delta\mathbf{A}_{p,\ell}$. Replacing $\mathbf{g}_{p,\ell}$ in (12) with $\widetilde{\mathbf{g}}_{p,\ell}$, the SINR is rewritten as

$$\text{SINR}_p \triangleq \frac{\sum_{\ell=0}^{L_p-1}\mathcal{L}_{p,\ell}|\widetilde{\mathbf{g}}_{p,\ell}^{\dagger}\mathbf{w}_p|^2}{\sum_{q\neq p}^{K}\sum_{\ell=0}^{L_p-1}\mathcal{L}_{p,\ell}|\widetilde{\mathbf{g}}_{p,\ell}^{\dagger}\mathbf{w}_q|^2 + \sigma_p^2}. \tag{20}$$

Consequently, the SCPM problem under the influence of phase uncertainties (SCPM-PU) follows

$$s.t. \quad \begin{cases} \underset{\{\mathbf{w}_p\}_{p=1}^K}{\arg\min} \sum_{p=1}^{K}\|\mathbf{w}_p\|^2 \\ \frac{1}{\gamma_0}\mathbf{w}_p^{\dagger}(\widetilde{\mathbf{Q}}_p + \Delta\widetilde{\mathbf{Q}}_p)\mathbf{w}_p \geq \\ \quad \sum_{q=1,q\neq p}^{K}\mathbf{w}_q^{\dagger}(\widetilde{\mathbf{Q}}_p + \Delta\widetilde{\mathbf{Q}}_p)\mathbf{w}_q + \sigma_p^2, \\ |\delta\psi_{(n,m)}^{(i)}| \leq \varepsilon, \\ \forall \ i \in \mathcal{I}_4, \ n \in \mathcal{I}_N, \ m \in \mathcal{I}_M, \ p \in \mathcal{I}_K \end{cases} \tag{21}$$

with $\widetilde{\mathbf{Q}}_p \triangleq \mathcal{L}_{p,0}\widetilde{\mathbf{g}}_{p,0}\widetilde{\mathbf{g}}_{p,0}^{\dagger}$ and $\widetilde{\Delta}\mathbf{Q}_p \triangleq \sum_{\ell=1}^{L_p-1}\mathcal{L}_{p,\ell}\widetilde{\mathbf{g}}_{p,\ell}\widetilde{\mathbf{g}}_{p,\ell}^{\dagger}$. We note that the error in $(\phi_{p,0},\theta_{p,0})$ can also be incorporated into $\delta\psi_{(n,m)}^{(i)}$, resulting in (21) as well with a similar procedure given above.

B. Robust BF Design to Combat Phase Uncertainties

The robust BF problem now becomes to design $\mathbf{w}_p$ that satisfy the SINR constraint for all $|\delta\psi_{(n,m)}^{(i)}| \leq \varepsilon$. Although there have been rich results in literatures which consider robust MU DL BF problems, most study BFer designs under the uncertainties in fading channel coefficients. Recent results in [42], [43] show that a least conservative and, hence, a power efficient robust BF method can be constructed using the S-Procedure [28] and semidefinite relaxation (SDR). Different from the existing results, we consider herein robust designs to combat the phase shifter errors. We will show in this section that the robust SCPM-PU problem of (21) can be reformulated as an SDP problem, making use of the S-Procedure as well. The results presented herein also lead to a more robust nonlinear formulation of BFer to be presented in Section V.

Continued from (19), by the Cauchy-Schwarz inequality and the upper bound $|\delta\psi_{(n,m)}^{(i)}| \leq \varepsilon$ on the phase uncertainties, the uncertainty in the RAF of (19) can be bounded from above by

$$\begin{aligned} \|\Delta A_{p,\ell}^{(i)}\| &\triangleq \|\left(\underline{\wp}_{p,\ell}^{(i)}\right)^{\dagger}\boldsymbol{\Delta}^{(i)}\| \\ &\leq \|\underline{\wp}_{p,\ell}^{(i)}\|\|\boldsymbol{\Delta}^{(i)}\| = \sqrt{MN}\epsilon, \forall \ |\delta\psi_{(n,m)}^{(i)}| \leq \varepsilon \end{aligned} \tag{22}$$

with the equality holding when $\boldsymbol{\Delta}^{(i)} \propto \underline{\wp}_{p,\ell}^{(i)}$. Therefore, by (10), (19) and (22), we have

$$\begin{aligned} \|\Delta\mathbf{g}_{p,\ell}\| &= \|E_{p,\ell}\mathbf{s}_{p,\ell}^{\dagger}\Delta\mathbf{A}_{p,\ell}\| \\ &\leq \sqrt{4MN}|E_{p,\ell}|\varepsilon \triangleq \epsilon_{p,\ell}, \ \forall \ |\delta\psi_{(n,m)}^{(i)}| \leq \varepsilon \end{aligned} \tag{23}$$

as $|\exp\{j(b_x^{(i)}\Psi_{x,p,\ell} + b_y^{(i)}\Psi_{y,p,\ell})\}| = 1$ for $\mathbf{s}_{p,\ell}$ in (10). Now rewrite the expression of (20) as what is shown in (24). This SINR expression can also lead to a R-SCPM problem in the forms of (15) and (16) if we redefine $\Delta\mathbf{Q}_p \triangleq \mathcal{L}_{p,0}(\Delta\mathbf{g}_{p,0}\Delta\mathbf{g}_{p,0}^{\dagger} + \Delta\mathbf{g}_{p,0}\mathbf{g}_{p,0}^{\dagger} + \mathbf{g}_{p,0}\Delta\mathbf{g}_{p,0}^{\dagger}) + \sum_{\ell=1}^{L_p-1}\mathcal{L}_{p,\ell}\widetilde{\mathbf{g}}_{p,\ell}\widetilde{\mathbf{g}}_{p,\ell}^{\dagger}$ in this case, and find a proper upper bound for $\|\Delta\mathbf{Q}_p\|_{\mathcal{F}}$, making use of (23).

$$\text{SINR}_p = \frac{\mathcal{L}_{p,0}|(\mathbf{g}_{p,0}+\Delta\mathbf{g}_{p,0})^\dagger\mathbf{w}_p|^2 + \sum_{\ell=1}^{L_p-1}\mathcal{L}_{p,\ell}|\widetilde{\mathbf{g}}_{p,\ell}^\dagger\mathbf{w}_p|^2}{\sum_{q\neq p}^{K}\left[\mathcal{L}_{p,0}|(\mathbf{g}_{p,0}+\Delta\mathbf{g}_{p,0})^\dagger\mathbf{w}_q|^2 + \sum_{\ell=1}^{L_p-1}\mathcal{L}_{p,\ell}|\widetilde{\mathbf{g}}_{p,\ell}^\dagger\mathbf{w}_q|^2\right] + \sigma_p^2}. \tag{24}$$

Specifically, redefine the Rician K-factor under the angle uncertainties of phase shifters as

$$\begin{aligned}\widetilde{\kappa}_p &\triangleq \frac{\mathcal{L}_{p,0}\|\widetilde{\mathbf{g}}_{p,0}\|^2}{\sum_{\ell=1}^{L_p-1}\mathcal{L}_{p,\ell}\|\widetilde{\mathbf{g}}_{p,\ell}\|^2} \\ &= \frac{\mathcal{L}_{p,0}|E_{p,0}|^2\sum_{i=1}^{4}|\widetilde{A}_{p,0}^{(i)}|^2}{\sum_{\ell=1}^{L_p-1}\mathcal{L}_{p,\ell}|E_{p,\ell}|^2\sum_{i=1}^{4}|\widetilde{A}_{p,\ell}^{(i)}|^2}\end{aligned} \tag{25}$$

and rewrite the ISI components of $\Delta\mathbf{Q}_p$ in terms of $\widetilde{\kappa}_p$ and the LOS component $\mathcal{L}_{p,0}\|\widetilde{\mathbf{g}}_{p,0}\|^2$. Then, applying (23), and the triangle and Cauchy-Schwarz inequalities to bound the effects of $\Delta\mathbf{g}_{p,0}$ in $\widetilde{\mathbf{g}}_{p,0}$, we will obtain an upper bound of $\|\Delta\mathbf{Q}_p\|_{\mathcal{F}} \leq \mathcal{L}_{p,0}(\epsilon_p^2+2\epsilon_p\|\mathbf{g}_{p,0}\|)+\frac{\mathcal{L}_{p,0}}{\widetilde{\kappa}_p}\|\widetilde{\mathbf{g}}_{p,0}\|^2$. [3]

Compared to the upper bound of $\|\Delta\mathbf{Q}_p\|_{\mathcal{F}} \leq \frac{1}{\kappa_p}\mathcal{L}_{p,0}\|\mathbf{g}_{p,0}\|^2$ for (15), the cross product terms between $\mathbf{g}_{p,0}$ and $\Delta\mathbf{g}_{p,0}$ make the upper bound $\mathcal{L}_{p,0}(\epsilon_p^2+2\epsilon_p\|\mathbf{g}_{p,0}\|)+\frac{\mathcal{L}_{p,0}}{\widetilde{\kappa}_p}\|\widetilde{\mathbf{g}}_{p,0}\|^2$ of $\|\Delta\mathbf{Q}_p\|_{\mathcal{F}}$, in this case, much higher due to the magnitudes of $2\epsilon_p\mathcal{L}_{p,0}\|\mathbf{g}_{p,0}\|$, in particular for LOS channels with high K-factors. The power of the resultant $\mathbf{w}_p$ to combat the uncertainty $\|\Delta\mathbf{Q}_p\|_{\mathcal{F}}$ thus becomes unacceptably high for a realistic system, making the method of (15) and (16) inappropriate for (24). To resolve this feasibility issue, we alternatively find a lower bound for (24) with (26) shown in the next page, by defining parameters $\widetilde{\mathcal{K}}_p \geq \frac{1}{\widetilde{\kappa}_p}\mathcal{L}_{p,0}(\|\mathbf{g}_{p,0}\|+\epsilon_p)^2$ to upper bound the effect of ISI in a sense of [4]

$$\begin{aligned}\|\Delta\widetilde{\mathbf{Q}}_p\|_{\mathcal{F}} &\leq \sum_{\ell=1}^{L_p-1}\|\mathcal{L}_{p,\ell}\widetilde{\mathbf{g}}_{p,\ell}\widetilde{\mathbf{g}}_{p,\ell}^\dagger\|_{\mathcal{F}} = \tfrac{1}{\widetilde{\kappa}_p}\mathcal{L}_{p,0}\|\widetilde{\mathbf{g}}_{p,0}\|^2 \\ &= \tfrac{1}{\widetilde{\kappa}_p}\mathcal{L}_{p,0}\|\mathbf{g}_{p,0}+\Delta\mathbf{g}_{p,0}\|^2 \leq \widetilde{\mathcal{K}}_p.\end{aligned} \tag{27}$$

Given $\widetilde{\mathcal{K}}_p$, it follows that $\underset{\|\Delta\widetilde{\mathbf{Q}}_p\|_{\mathcal{F}}\leq\widetilde{\mathcal{K}}_p}{\arg\max}\sum_{q\neq p}^{K}\mathbf{w}_q^\dagger\Delta\widetilde{\mathbf{Q}}_p\mathbf{w}_q$ *s.t.* $\Delta\widetilde{\mathbf{Q}}_p \succeq \mathbf{0}$ yields $\Delta\widetilde{\mathbf{Q}}_p = \widetilde{\mathcal{K}}_p\frac{\sum_{q\neq p}^{K}\mathbf{w}_q\mathbf{w}_q^\dagger}{\|\sum_{q\neq p}^{K}\mathbf{w}_q\mathbf{w}_q^\dagger\|_{\mathcal{F}}}$, and $\min_{\|\Delta\widetilde{\mathbf{Q}}_p\|_{\mathcal{F}}\leq\widetilde{\mathcal{K}}_p}\mathbf{w}_p^\dagger\Delta\widetilde{\mathbf{Q}}_p\mathbf{w}_p = 0$ as $\Delta\widetilde{\mathbf{Q}}_p \succeq \mathbf{0}$. Substituting these values back into (26), and bounding the result with a lower limit γ_0 such that $\min_{\|\Delta\widetilde{\mathbf{Q}}_p\|_{\mathcal{F}}\leq\widetilde{\mathcal{K}}_p}\text{SINR}_p \geq \gamma_0$, we will obtain

$$\begin{aligned}(\mathbf{g}_{p,0}+\Delta\mathbf{g}_{p,0})^\dagger\left(\tfrac{\mathcal{L}_{p,0}}{\gamma_0}\mathbb{W}_p - \mathcal{L}_{p,0}\sum_{q\neq p}^{K}\mathbb{W}_q\right)(\mathbf{g}_{p,0}+\Delta\mathbf{g}_{p,0}) \\ -\sigma_p^2 \geq \widetilde{\mathcal{K}}_p\left\|\sum_{q\neq p}^{K}\mathbb{W}_q\right\|_{\mathcal{F}}\end{aligned} \tag{28}$$

with $\mathbb{W}_p \triangleq \mathbf{w}_p\mathbf{w}_p^\dagger$. A valid solution, thus, must satisfy $\mathbb{W}_p \succeq \mathbf{0}$ and $\text{rank}\{\mathbb{W}_p\} = 1$, $\forall p \in \mathcal{I}_K$.

[3]For simplicity, we have $\epsilon_p \equiv \epsilon_{p,0}$ since only $\epsilon_{p,0}$ in the LOS direction will be used hereafter.

[4]The values of $\widetilde{\mathcal{K}}_p$ are set as $\frac{1}{\kappa}\mathcal{L}_{p,0}\|\mathbf{g}_{p,0}+\epsilon_p\|^2$ in simulations, with κ being the lower bound for $\widetilde{\kappa}_p$, $\forall p \in \mathcal{I}_K$.

Now, introducing some parameters $\tau_p \geq 0$, $\forall p \in \mathcal{I}_K$, that satisfy

$$\begin{aligned}(\mathbf{g}_{p,0}+\Delta\mathbf{g}_{p,0})^\dagger\left(\tfrac{1}{\gamma_0}\mathbb{W}_p - \sum_{q\neq p}^{K}\mathbb{W}_q\right)(\mathbf{g}_{p,0}+\Delta\mathbf{g}_{p,0}) - \\ \tfrac{\sigma_p^2}{\mathcal{L}_{p,0}} \geq \tau_p \geq \tfrac{\widetilde{\mathcal{K}}_p}{\mathcal{L}_{p,0}}\left\|\sum_{q\neq p}^{K}\mathbb{W}_q\right\|_{\mathcal{F}}\end{aligned} \tag{29}$$

we then obtain from above the constraints that satisfy $\text{SINR}_p \geq \min_{\|\Delta\widetilde{\mathbf{Q}}_p\|_{\mathcal{F}}\leq\widetilde{\mathcal{K}}_p}\text{SINR}_p \geq \gamma_0$ according to (24) and (26). Making use of the fact that $\left\|\sum_{q\neq p}^{K}\mathbb{W}_q\right\|_{\mathcal{F}} \geq \sum_{q\neq p}^{K}\|\mathbb{W}_q\|_{\mathcal{F}}$, we eventually obtain an alternative set of constraints for the robust SCPM-PU problem of (21), given by

$$\begin{aligned}(\mathbf{g}_{p,0}+\Delta\mathbf{g}_{p,0})^\dagger\left(\tfrac{1}{\gamma_0}\mathbb{W}_p - \sum_{q\neq p}^{K}\mathbb{W}_q\right)(\mathbf{g}_{p,0}+\Delta\mathbf{g}_{p,0}) - \\ \tfrac{\sigma_p^2}{\mathcal{L}_{p,0}} \geq \tau_p \geq \tfrac{\widetilde{\mathcal{K}}_p}{\mathcal{L}_{p,0}}\sum_{q\neq p}^{K}\|\mathbb{W}_q\|_{\mathcal{F}}.\end{aligned} \tag{30}$$

This constraint formulation allows us to handle the phase uncertainties in $\Delta\mathbf{g}_{p,0}$ and ISI of (24), separately. Nevertheless, to make (29) and (30) hold under the condition of (23), it requires

$$\begin{aligned}(\mathbf{g}_{p,0}+\Delta\mathbf{g}_{p,0})^\dagger\left(\tfrac{1}{\gamma_0}\mathbb{W}_p - \sum_{q\neq p}^{K}\mathbb{W}_q\right)(\mathbf{g}_{p,0}+\Delta\mathbf{g}_{p,0}) - \\ \tfrac{\sigma_p^2}{\mathcal{L}_{p,0}} \geq \tau_p,\ \forall\ \epsilon_p^{-2}\|\Delta\mathbf{g}_{p,0}\|^2 \leq 1.\end{aligned} \tag{31}$$

These infinite many inequalities, however, can be transformed into few linear matrix inequalities (LMIs), making use of the S-Procedure [28], [43]. Specifically, define an LMI of the form

$$\begin{aligned}&\Omega_p(\mathbb{W}_1,\ldots,\mathbb{W}_K,\tau_p,\zeta_p) \\ &\triangleq \begin{bmatrix}\mathbf{I}_4 \\ \mathbf{g}_{p,0}^\dagger\end{bmatrix}\left(\tfrac{1}{\gamma_0}\mathbb{W}_p - \sum_{q\neq p}^{K}\mathbb{W}_q\right)\begin{bmatrix}\mathbf{I}_4 & \mathbf{g}_{p,0}\end{bmatrix} + \\ &\begin{bmatrix}\frac{\zeta_p}{\epsilon_p^2}\mathbf{I}_4 & \mathbf{0} \\ \mathbf{0} & -\frac{\sigma_p^2}{\mathcal{L}_{p,0}}-\tau_p-\zeta_p\end{bmatrix} \succeq \mathbf{0}.\end{aligned} \tag{32}$$

The inequalities of (31) hold true if and only if there exist $\zeta_p \geq 0$ such that $\Omega_p(\mathbb{W}_1,\ldots,\mathbb{W}_K,\tau_p,\zeta_p) \succeq \mathbf{0}$, $\forall p \in \mathcal{I}_K$. Therefore, the robust SCPM-PU problem of (21) can be transformed with (30) and (31) into a power minimization problem subject to the LMI constraints of (32) and $\text{rank}\{\mathbb{W}_p\} = 1$, $\forall p \in \mathcal{I}_K$. Relaxing the constraints of $\text{rank}\{\mathbb{W}_p\} = 1$, the robust SCPM-PU problem essentially becomes an SDP problem, denoted by SDP-R-SCPM-PU, and is reformulated

$$\min_{\|\Delta\widetilde{\mathbf{Q}}_p\|_{\mathcal{F}}\le\widetilde{\mathcal{K}}_p}\text{SINR}_p \ge \frac{\mathcal{L}_{p,0}|\widetilde{\mathbf{g}}_{p,0}^{\dagger}\mathbf{w}_p|^2+\min\limits_{\|\Delta\widetilde{\mathbf{Q}}_p\|_{\mathcal{F}}\le\widetilde{\mathcal{K}}_p}\mathbf{w}_p^{\dagger}\Delta\widetilde{\mathbf{Q}}_p\mathbf{w}_p}{\sum_{q\ne p}^{K}\mathcal{L}_{p,0}|\widetilde{\mathbf{g}}_{p,0}^{\dagger}\mathbf{w}_q|^2+\max\limits_{\|\Delta\widetilde{\mathbf{Q}}_p\|_{\mathcal{F}}\le\widetilde{\mathcal{K}}_p}\sum_{q\ne p}^{K}\mathbf{w}_q^{\dagger}\Delta\widetilde{\mathbf{Q}}_p\mathbf{w}_q+\sigma_p^2} \tag{26}$$

in the form of

$$\begin{aligned}&\underset{\{\mathbb{W}_p,\tau_p,\zeta_p\}_{p=1}^K}{\arg\min}\ \sum_{p=1}^K\text{Tr}\{\mathbb{W}_p\}\\ s.t.\quad&\begin{cases}\Omega_p(\mathbb{W}_1,\ldots,\mathbb{W}_K,\tau_p,\zeta_p)\succeq\mathbf{0} & ,\zeta_p\ge 0,\\ \tau_p\mathcal{L}_{p,0}\ge\widetilde{\mathcal{K}}_p\sum\limits_{q\ne p}^{K}\|\mathbb{W}_q\|_{\mathcal{F}} & ,\mathbb{W}_p\succeq\mathbf{0},\\ \forall p\in\mathcal{I}_K.\end{cases}\end{aligned} \tag{33}$$

The complexity order for solving (33) is $\mathcal{O}(K^3 4^3)$, $K\le 4$, per iteration if using the interior-point method [44]. Simulations with CVX [36] show that $\text{rank}\{\widehat{\mathbb{W}}_p\}=1$ for all the optimal $\widehat{\mathbb{W}}_p$ even if the constraints of $\text{rank}\{\mathbb{W}_p\}=1$ have been relaxed in (33). This observation agrees with those reported in [42], [43], though a rigorous proof is required to justify the outcomes of our simulations.

We note that (30), and hence (33), will degenerate into another robust SCPM problem of

$$\begin{aligned}&\underset{\{\mathbf{w}_p\}_{p=1}^K}{\arg\min}\sum_{p=1}^K\|\mathbf{w}_p\|^2\\ s.t.\quad&\tfrac{1}{\gamma_0}\mathbf{w}_p^{\dagger}\mathbf{Q}_p\mathbf{w}_p-\sum_{q=1,q\ne p}^{K}\mathbf{w}_q^{\dagger}\left(\mathbf{Q}_p+\mathcal{K}_p\mathbf{I}\right)\mathbf{w}_q\ge\sigma_p^2,\\ &\forall p\in\mathcal{I}_K\end{aligned} \tag{34}$$

since $\mathbb{W}_p\triangleq\mathbf{w}_p\mathbf{w}_p^{\dagger}$, $\mathbf{Q}_p\triangleq\mathcal{L}_{p,0}\mathbf{g}_{p,0}\mathbf{g}_{p,0}^{\dagger}$, and $\Delta\mathbf{g}_{p,0}=\mathbf{0}$ when $\varepsilon=0$. This is essentially a QCQP problem and has closed-form solutions of $\mathbf{w}_p$ [34]. For convenience, this criterion is denoted by QCQP-R-SCPM, and will be used to justify the effectiveness of (26) in comparison with (15).

Furthermore, when κ_p are very large, we may set $\mathcal{K}_p=0$, the optimal $\mathbf{w}_p$ then degenerate to a decorrelating precoder (DP) [37]. Specifically, put the received signals of (9), $\forall p\in\mathcal{I}_K$, into a vector form of $\text{diag}\{h_{1,0},\ldots,h_{K,0}\}\mathbf{G}_0\mathbf{W}\mathbf{x}$ with $\mathbf{G}_0\triangleq[\sqrt{\mathcal{L}_{1,0}}E_{1,0}^*\mathbf{A}_{1,0}^{\dagger}\mathbf{s}_{1,0},\ldots,\sqrt{\mathcal{L}_{K,0}}E_{K,0}^*\mathbf{A}_{K,0}^{\dagger}\mathbf{s}_{K,0}]^{\dagger}$. The problem of (34) will return a DP of the form

$$\mathbf{W}\triangleq\sqrt{\gamma_0}\mathbf{G}_0^{\dagger}\left(\mathbf{G}_0\mathbf{G}_0^{\dagger}\right)^{-1}\text{diag}\left\{\left[\frac{\sigma_1}{\sqrt{\mathcal{L}_{1,0}}},\ldots,\frac{\sigma_K}{\sqrt{\mathcal{L}_{K,0}}}\right]\right\} \tag{35}$$

when $\mathcal{K}_p=0$, $\forall p\in\mathcal{I}_K$. The power consumption is, thus, $\mathcal{P}_0\triangleq\text{Tr}\{\mathbf{W}^{\dagger}\mathbf{W}\}$. This ideal BFer is used as a benchmark in simulations to evaluate the effectiveness of the proposed robust criteria.

V. A Nonlinear Programming Method for Robust BF Design

Though elegant, the SDP-R-SCPM-PU criterion of (33) still requires a numerical solver to carry out $\mathbb{W}_p$. To improve the feasibility in practical implementations, we are interested in closed-form or semi closed-form expressions of $\mathbf{w}_p$. Observe from (19). If we define $\nu_{p,q},\ p,q\in\mathcal{I}_K$, such that

$$|\mathbf{g}_{p,0}^{\dagger}\mathbf{w}_q|\le\nu_{p,q}\|\mathbf{g}_{p,0}\|\|\mathbf{w}_q\| \tag{36}$$

then the LOS signal power $|\widetilde{\mathbf{g}}_{p,0}^{\dagger}\mathbf{w}_p|^2$ in (20) can be lower bounded by a function of $\mathbf{w}_p$, given by

$$\begin{aligned}|\widetilde{\mathbf{g}}_{p,0}^{\dagger}\mathbf{w}_p|^2 &\ge (|\mathbf{g}_{p,0}^{\dagger}\mathbf{w}_p|-|\Delta\mathbf{g}_{p,0}^{\dagger}\mathbf{w}_p|)^2\\ &\ge \left(|\mathbf{g}_{p,0}^{\dagger}\mathbf{w}_p|-\epsilon_p\|\mathbf{w}_p\|\right)^2\\ &\ge |\mathbf{g}_{p,0}^{\dagger}\mathbf{w}_p|^2+\epsilon_p^2\|\mathbf{w}_p\|^2-2\epsilon_p\nu_{p,p}\|\mathbf{g}_{p,0}\|\|\mathbf{w}_p\|^2\\ &\triangleq \mathbf{w}_p^{\dagger}[\mathbf{g}_{p,0}\mathbf{g}_{p,0}^{\dagger}+\xi_{p,p}\mathbf{I}]\mathbf{w}_p\end{aligned} \tag{37}$$

where $\xi_{p,p}\triangleq\epsilon_p\left(\epsilon_p-2\nu_{p,p}\|\mathbf{g}_{p,0}\|\right)$, provided that $|\mathbf{g}_{p,0}^{\dagger}\mathbf{w}_p|\ge\epsilon_p\|\mathbf{w}_p\|$. On the contrary, the LOS interference power $|\widetilde{\mathbf{g}}_{p,0}^{\dagger}\mathbf{w}_q|^2$ in (20) can be upper bounded by a function of $\mathbf{w}_q$ that follows

$$\begin{aligned}|\widetilde{\mathbf{g}}_{p,0}^{\dagger}\mathbf{w}_q|^2 &\le (|\mathbf{g}_{p,0}^{\dagger}\mathbf{w}_q|+|\Delta\mathbf{g}_{p,0}^{\dagger}\mathbf{w}_q|)^2\\ &\le (|\mathbf{g}_{p,0}^{\dagger}\mathbf{w}_q|+\epsilon_p\|\mathbf{w}_q\|)^2\\ &\le |\mathbf{g}_{p,0}^{\dagger}\mathbf{w}_q|^2+\epsilon_p^2\|\mathbf{w}_q\|^2+2\epsilon_p\nu_{p,q}\|\mathbf{g}_{p,0}\|\|\mathbf{w}_q\|^2\\ &\triangleq \mathbf{w}_q^{\dagger}[\mathbf{g}_{p,0}\mathbf{g}_{p,0}^{\dagger}+\xi_{p,q}\mathbf{I}]\mathbf{w}_q\end{aligned} \tag{38}$$

where $\xi_{p,q}\triangleq\epsilon_p\left(\epsilon_p+2\nu_{p,q}\|\mathbf{g}_{p,0}\|\right)$ for $p,q\in\mathcal{I}_K$ and $p\ne q$. Therefore, the signal components in (30) for robust HBF can be bounded from below by a quadratic function of $\mathbf{w}_p$ in the form of

$$\begin{aligned}&\frac{1}{\gamma_0}|\widetilde{\mathbf{g}}_{p,0}^{\dagger}\mathbf{w}_p|^2-\sum_{q\ne p}^{K}|\widetilde{\mathbf{g}}_{p,0}^{\dagger}\mathbf{w}_q|^2\\ &\qquad\ge\frac{1}{\gamma_0}\mathbf{w}_p^{\dagger}\left[\mathbf{g}_{p,0}\mathbf{g}_{p,0}^{\dagger}+\xi_{p,p}\mathbf{I}\right]\mathbf{w}_p-\\ &\qquad\qquad\sum_{q\ne p}^{K}\mathbf{w}_q^{\dagger}\left[\mathbf{g}_{p,0}\mathbf{g}_{p,0}^{\dagger}+\xi_{p,q}\mathbf{I}\right]\mathbf{w}_q.\end{aligned} \tag{39}$$

This inequality bounds the first term of (30) and (31) from below with a quadratic function of $\mathbf{w}_p$. Nonetheless, the parameters $\nu_{p,q}$ introduced in (36) make (39) in fact a high-order nonlinear inequality. Therefore, to satisfy both (30) and (31), the robust SCPM-PU criterion of (21) is transformed by (39) into a more conservative nonlinear programming (NLP) problem of the form

$$\begin{aligned}&\underset{\{\mathbf{w}_p,\ \nu_{k,p}\}_{k,p=1}^K}{\arg\min}\ \sum_{p=1}^K\|\mathbf{w}_p\|^2\\ s.t.\quad&\begin{cases}\frac{1}{\gamma_0}\mathbf{w}_p^{\dagger}\left[\mathbf{g}_{p,0}\mathbf{g}_{p,0}^{\dagger}+\xi_{p,p}\mathbf{I}\right]\mathbf{w}_p-\\ \sum\limits_{q\ne p}^{K}\mathbf{w}_q^{\dagger}\left[\mathbf{g}_{p,0}\mathbf{g}_{p,0}^{\dagger}+(\xi_{p,q}+\frac{\widetilde{\mathcal{K}}_p}{\mathcal{L}_{p,0}})\mathbf{I}\right]\mathbf{w}_q\ge\frac{\sigma_p^2}{\mathcal{L}_{p,0}}\\ |\mathbf{g}_{p,0}^{\dagger}\mathbf{w}_q|^2\le\nu_{p,q}^2\|\mathbf{g}_{p,0}\|^2\|\mathbf{w}_q\|^2,\ \nu_{p,q}>0,\\ \forall p,q,k\in\mathcal{I}_K.\end{cases}\end{aligned} \tag{40}$$

This optimization problem, denoted by NLP-R-SCPM-PU, will be shown to be convex in the appendix when $\nu_{p,q}>0,\ \forall p,q\in\mathcal{I}_K$. The optimal $\nu_{p,q}$ and $\mathbf{w}_p$ can thus be solved based on the Karush-Kuhn-Tucker (K.K.T.) conditions of (40)

[28]. The procedure for solving this problem is summarized in the following theorem. Despite the optimality, the equalities for the lower (37) and the upper (38) bounds in (39) in general do not hold for the same $\Delta\mathbf{g}_{p,0}$ simultaneously, which will otherwise require $\Delta\mathbf{g}_{p,0} \propto \mathbf{g}_{p,0} \propto \mathbf{w}_p \propto \mathbf{w}_q$, $\forall q \neq p$. This property makes the formulation of (40) more conservative than that of (33), however, provides extra robustness against the MAI in (26) from which both (33) and (40) are derived, when $\widetilde{\mathcal{K}}_p$ are not set high enough to combat ISI.

Theorem 1: Consider the problem of (40). Suppose that $\exists$ $\lambda_p > 0$, $\lambda_p \in \mathcal{R}$, $\forall p \in \mathcal{I}_K$ such that

$$\frac{1}{\lambda_p} = \frac{1}{\gamma_0}\eta_{p,p}\mathbf{g}_{p,0}^{\dagger}\mathbf{T}_{p,p}^{-1}\mathbf{g}_{p,0} \tag{41}$$

and $\exists\ \frac{\epsilon_p}{\|\mathbf{g}_{p,0}\|} \leq \nu_{p,p} \leq 1$ and $0 \leq \nu_{p,q} \leq 1$, $p \neq q$, $\forall p, q \in \mathcal{I}_K$, that satisfy

$$\frac{1}{\nu_{p,p}} = \frac{\lambda_p}{\gamma_0}\eta_{p,p}\|\mathbf{g}_{p,0}\|\left\|\mathbf{T}_{p,p}^{-1}\mathbf{g}_{p,0}\right\| \tag{42}$$

$$\frac{1}{\nu_{q,p}} = \lambda_q\eta_{q,p}\|\mathbf{g}_{q,0}\|\left\|\mathbf{T}_{q,p}^{-1}\mathbf{g}_{q,0}\right\|, \forall q \neq p \tag{43}$$

where $\eta_{p,p} \triangleq 1 - \frac{\epsilon_p}{\|\mathbf{g}_{p,0}\|\nu_{p,p}}$, $\eta_{q,p} \triangleq 1 + \frac{\epsilon_q}{\|\mathbf{g}_{q,0}\|\nu_{q,p}}$, $\mathbf{T}_{p,p} \triangleq \alpha_p\mathbf{I} + \sum_{q\neq p}^{K}\lambda_q\eta_{q,p}\mathbf{g}_{q,0}\mathbf{g}_{q,0}^{\dagger}$ and $\mathbf{T}_{q,p} \triangleq \alpha_p\mathbf{I} + \sum_{k\neq p,q}^{K}\lambda_k\eta_{k,p}\mathbf{g}_{k,0}\mathbf{g}_{k,0}^{\dagger} - \frac{\lambda_p}{\gamma_0}\eta_{p,p}\mathbf{g}_{p,0}\mathbf{g}_{p,0}^{\dagger}$ with $\alpha_p \triangleq 1 - \frac{\lambda_p}{\gamma_0}\epsilon_p(\epsilon_p - \nu_{p,p}\|\mathbf{g}_{p,0}\|) + \sum_{q\neq p}^{K}\lambda_q(\epsilon_q(\epsilon_q + \nu_{q,p}\|\mathbf{g}_{q,0}\|) + \frac{\widetilde{\mathcal{K}}_q}{\mathcal{L}_{q,0}})$. Define a $K \times K$ matrix $\mathbf{F}$ whose entries are given by

$$F_{p,p} \triangleq \frac{\lambda_p^2}{\gamma_0^3}\eta_{p,p}^2\left(\left|\mathbf{g}_{p,0}^{\dagger}\mathbf{T}_{p,p}^{-1}\mathbf{g}_{p,0}\right|^2 + \xi_{p,p}\left\|\mathbf{T}_{p,p}^{-1}\mathbf{g}_{p,0}\right\|^2\right) \tag{44}$$

$$F_{p,q} \triangleq -\frac{\lambda_q^2}{\gamma_0^2}\eta_{q,q}^2\left(\left|\mathbf{g}_{p,0}^{\dagger}\mathbf{T}_{q,q}^{-1}\mathbf{g}_{q,0}\right|^2 + \xi_{p,q}\left\|\mathbf{T}_{q,q}^{-1}\mathbf{g}_{q,0}\right\|^2\right) \tag{45}$$

$\forall p, q \in \mathcal{I}_K$, $p \neq q$. If $\mathbf{F} \succ \mathbf{0}$, then the program is strictly feasible. Define $\Upsilon \triangleq [\frac{\sigma_1^2}{\mathcal{L}_{1,0}}, \ldots, \frac{\sigma_K^2}{\mathcal{L}_{K,0}}]^T$ and $\Gamma \triangleq [\chi_1^2, \ldots, \chi_K^2]^T = \mathbf{F}^{-1}\Upsilon$. Let χ_p be the positive real root of χ_p^2. The optimal BF wights $\widehat{\mathbf{w}}_p$ are given by

$$\widehat{\mathbf{w}}_p = \chi_p\frac{\lambda_p}{\gamma_0}\eta_{p,p}\mathbf{T}_{p,p}^{-1}\mathbf{g}_{p,p}. \tag{46}$$

And the minimum power consumption is $\mathcal{P}_0 = \sum_{p=1}^{K}\frac{\lambda_p\sigma_p^2}{\mathcal{L}_{p,0}}$. The proof is provided in the appendix.

Compared to the SDP-R-SCPM-PU criterion of (33), Theorem 1 provides an algorithm whose complexity is one order lower at $\mathcal{O}(K^2 4^3)$ per iteration, and whose closed-from expressions are more friendly for implementations. The optimal λ_p and $\nu_{q,p}$ can be solved iteratively with an inner loop to update $\nu_{q,p}$, $\forall p, q \in \mathcal{I}_K$, with (42) and (43), followed by an outer loop to update λ_p of (41), based on the fixed-point principle. In a special case of $K = 2$, (41) can be rewritten as

$$\alpha_p\left(\alpha_p - \frac{\lambda_p}{\gamma_0}\eta_{p,p}\|\mathbf{g}_{p,0}\|^2 + \lambda_q\eta_{q,p}\|\mathbf{g}_{q,0}\|^2\right) = \frac{1}{\gamma_0}\eta_{p,p}\eta_{q,p}\lambda_p\lambda_q\left(\|\mathbf{g}_{p,0}\|^2\|\mathbf{g}_{q,0}\|^2 - |\mathbf{g}_{p,0}^{\dagger}\mathbf{g}_{q,0}|^2\right) \tag{47}$$

which can be further expressed as a quadratic function of λ_p or λ_q, and, hence, solved immediately given $\nu_{p,p}$, $\nu_{q,p}$ and λ_q or λ_p, respectively, of the previous iteration. On the other hand, (42) can be reformulated as a quartic function in $\nu_{p,p}$ given λ_p, λ_q and $\nu_{q,p}$, $q \neq p$, and so can (43) as a quartic function of $\nu_{q,p}$ given λ_p, λ_q and $\nu_{p,p}$. Therefore, they can be solved in closed forms [45].

The feasibility for (40) depends on the convergency of the iterations between (41) $\sim$ (43), which are closely related to the upper bound of the phase uncertainty, ε, (*c.f.* (23)). The influences of ε on the performance of (33) and (40) will be jointly studied by simulations in the next section.

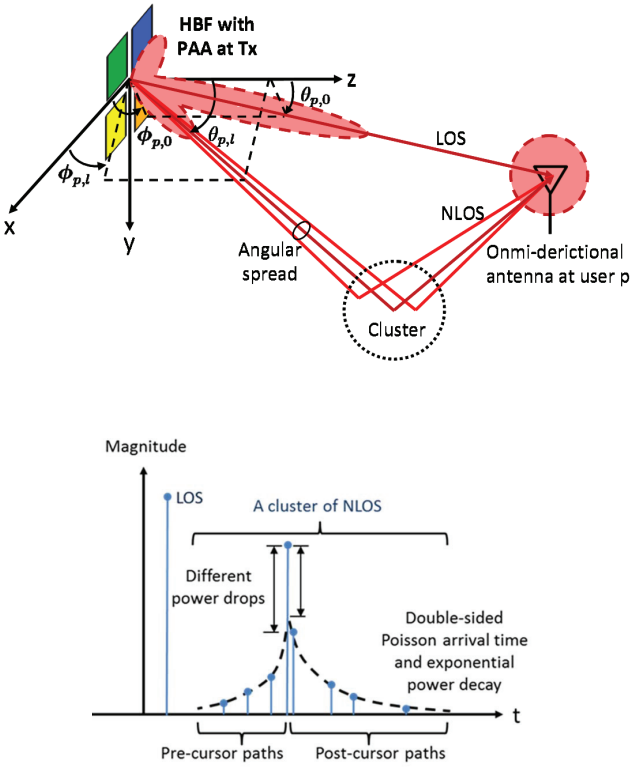

Fig. 4. An illustration of indoor 60 GHz multi-cluster channels. Left plot shows the LOS path and the NLOS reflection rays in a cluster. Right plot shows the average power versus the arrival time of the rays.

VI. Simulation Studies

Performance of the HBF schemes is evaluated in terms of its transmit power $\sum_{p=1}^{K}\|\mathbf{w}_p\|^2$, and the *SINR satisfaction ratio* defined as the percentage in which all users' SINR constraints are satisfied out of the simulated channels. The channels are simulated in an indoor environment as illustrated in Fig. 1(b) based on the models developed for IEEE 802.11ad [3], [32] and 802.15.3c [38], with the transmit antenna's pattern replaced by the HBF pattern of (6), and the receive antenna assumed an omnidirectional antenna. The simulation setting and the dimension of the patch antenna are the same to what describe in Section III-A and Section II-A, respectively, with $d_x = d_y = 2.5$ mm in Fig. 2(b). Since the performance of a scheme is closely related to the K-factor of the channel, and vary in different locations due to power propagation and NLOS reflection losses, we start by introducing some details of the channel models used in simulations.

A. Baseband Channel Model for Indoor 60 GHz Radio

The propagation channel of 60 GHz radio is a multi-cluster channel as illustrated in Fig. 4. For the LOS path, the traveling distance and the angle of departure (AoD) are deterministic, while for NLOS paths, only the AoD and the corresponding reflection angle, and hence the traveling distance, of a cluster of rays are deterministic. By the principle of reflection, a receiver may have at most 16 incoming clusters from the first and second reflections between walls and the ceiling.

The AoD of a ray is Gaussian distributed with mean equal to the AoD of its cluster and variances equal to $(5^\circ)^2$ in both ϕ and θ. As for the time of arrival (ToA) of a ray, it may be less or greater than the ToA of its cluster. Therefore, the rays of a cluster are divided into pre-cursor and post-cursor groups whose ToAs are backward and forward Poisson distributed with respect to (*w.r.t.*) the ToA of their cluster. There are 6 pre-cursor and 8 post-cursor rays in each cluster, according to the model of [32]. Their arrival rates equal 0.37 ns^{-1} and 0.31 ns^{-1}, respectively.

The power decay of a ray, ℓ, is a function of is its ToA, τ_ℓ, relative to the center of its cluster, and is expressed as $10^{-\frac{C_K}{10}}\exp\{-\frac{2|\tau_\ell|}{\varsigma}\}$ normalized by $\sum_{\ell=1}^{14} 10^{-\frac{C_K}{10}}\exp\{-\frac{2|\tau_\ell|}{\varsigma}\}$, with $C_K = 10$ and $\varsigma = 3.7$ ns for pre-cursor rays, and $C_K = 14.2$ and $\varsigma = 4.5$ ns for post-cursor rays. Multiplying this power decay by the hybrid array gain, $\widetilde{H}_q(\phi_{p,\ell}, \theta_{p,\ell})$, (19) in the direction of the ray, and by the receive power at the center of its cluster as well, yield the receive power of the ray.

The receive power at the center of a cluster is jointly determined by the pathloss $(\lambda/(4\pi D))^2$ along its traveling distance, D, the reflection losses and shadowing effects. The logarithms of reflection losses are truncated Gaussian distributed, with mean and standard deviation equal to 10 dB and 4 dB, respectively, for the first-order reflections, and 16 dB and 5 dB, respectively, for the second-order reflections. The logarithm of the shadowing effect is, however, Gaussian distributed with zero mean and standard deviation equal to 3.3 dB. Finally, the thermal noise variance at the receiver is equal to -83.9 dBm for 1 GHz BW at 25°C ambient temperature.

B. Simulation Results and Discussions

Based on the simulation setting described above, the K-factors of users 1 and 2 have been shown in Table I when $(x_T, z_T) = (5, 1)$, $(x_1, z_1) = (7, 5)$ and user 2 in different locations of Fig. 1(b). In the sequel, we choose for user 2 the opposite location *w.r.t.* $x = 5$ from user 1, namely $(x_2, z_2) = (2, 5)$, to examine the performance of proposed schemes if not particularly specified.

Fig. 5 compares SINR satisfaction ratios and power consumptions of using the type I and II partitions for PAA. The resolution of phase shifters, namely N_p, is assumed infinite. Nevertheless, for the HBF criteria of SDP-R-SCPM-PU (33) and SCPM-PU (21), we set $\varepsilon = 3^\circ$, while for the criteria of QCQP-R-SCPM (34), SDP-R-SCPM (16) and SCPM (13) that do not consider phase uncertainties, we set $\varepsilon = 0^\circ$. The lower bound, κ, for $\widetilde{\kappa}_p$ (25) and κ_p (14) is set equal to 100.

Consider the criterion of SDP-R-SCPM-PU, the type I partition consumes more power than the type II to achieve the same target SINR, γ_0, while the satisfaction ratios of these two are very close. The same situation happens to QCQP-R-SCPM as well, even if the satisfaction ratio of the type II is slightly higher in this case. This implies that MAI due to the grating lobes in the RAFs of the type II partition can be suppressed with its BB BFers $\mathbf{w}_p$ which do not have grating lobes in their BAFs. While there is no further mechanism to suppress the grating lobes in the BAFs of $\mathbf{w}_p$ in the type I partition. On the other hand, comparing the performance of the QCQP-R-SCPM and SDP-R-SCPM criteria for the type II partition, the satisfaction ratio of QCQP-R-SCPM is better, though their power consumptions are indistinguishable. This shows that the more conservative formulation of (26) from which SDP-R-SCPM-PU, and QCQP-R-SCPM as well when $\varepsilon = 0$, are derived provides some advantages in combating MAI and ISI, compared to that of (15) from which SDP-R-SCPM is obtained. This may explain why the satisfaction ratio of SDP-R-SCPM-PU is even higher than the others. Though originally developed to combat phase uncertainties, the more conservative formulation of SDP-R-SCPM-PU helps improve its satisfaction ratio as well. The improvement is 10% with only 1 dB more in power consumption, compared to the criterion of QCQP-R-SCPM for $\gamma_0 \leq 15$ dB. In contrast, the satisfaction ratios of using the DP of (35) are also shown in the figure, with their powers, $\mathcal{P}_0$, scaled up to that of QCQP-R-SCPM and SDP-R-SCPM-PU, denoted by DP and DP-PU in Fig. 5(a), respectively.

As a short summary, the extra power required to combat ISI or phase uncertainties is around 1 to 5 dB when $\gamma_0 \leq 15$ dB,

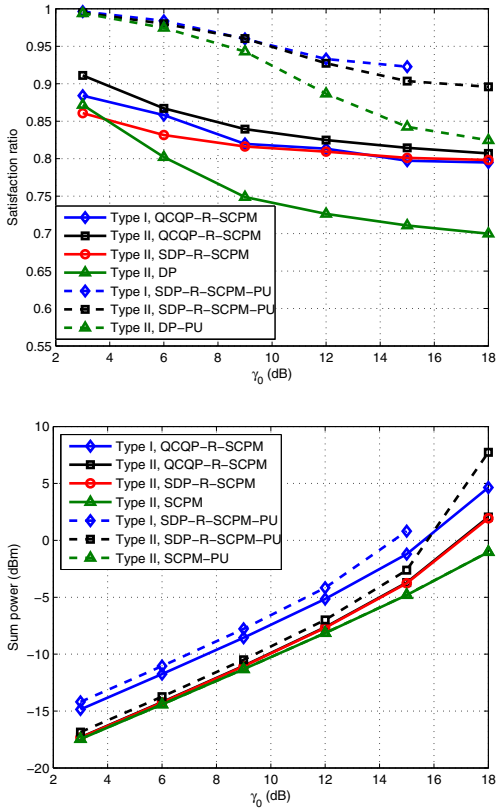

Fig. 5. SINR satisfaction ratios and power consumptions versus γ_0 for the type I and II partitions in Fig. 2.

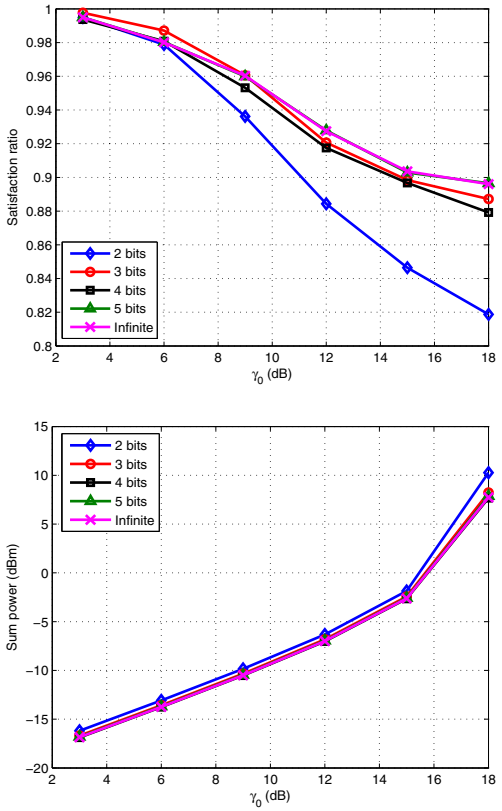

Fig. 6. SINR satisfaction ratios and power consumptions for different resolutions in phase shifters.

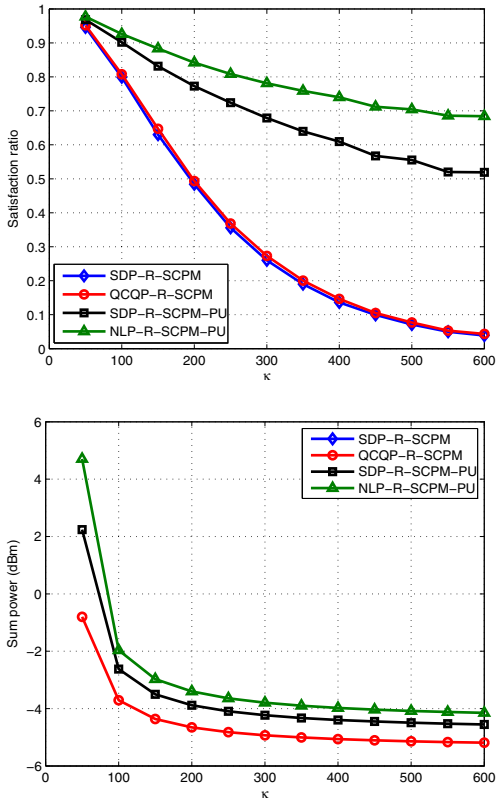

Fig. 7. SINR satisfaction ratios and power consumptions versus κ when $\gamma_0 = 15$ dB.

compared to SCPM (13) or SCPM-PU (21), respectively, that require perfect knowledge on ISI or phase errors. In addition, the type II partition gives a 3 dB gain in power consumption even if its implementation is more challenging from a circuit realization point of view. In the sequel, for succinctness, we only present the results for the type II partition.

Fig. 6 examines the influences of phase resolutions with the criterion of SDP-R-SCPM-PU (33) when $\varepsilon = 3^\circ$. The performance seems barely affected when $N_p \geq 8$, namely 3 bits in resolution. Nevertheless, the performance with $N_p = 8$ does slightly outperform that with phase shifters of infinite resolution when $\gamma_0 < 9$ dB. This echoes our argument at the end of Section II-B that a full HBF design such as (7) can be nontrivial. Since the advantage is minor here and the resolution of $N_p \geq 8$ is commonly available in designs such as [8], [10], for succinctness, we discuss only the influences of phase uncertainties in the sequel, and assume N_p to be infinite.

Fig. 7 shows the SINR satisfaction ratios and the sum powers versus different lower bounds, κ, for κ_p and $\widetilde{\kappa}_p$. The target SINR is set at $\gamma_0 = 15$ dB. For the criteria of SDP-R-SCPM (16) and QCQP-R-SCPM (34), we have $\varepsilon = 0^\circ$, while for the SDP-R-SCPM-PU (33) and NLP-R-SCPM-PU (40) criteria, we have $\varepsilon = 3^\circ$. Apparently, the satisfaction ratios of SDP-R-SCPM-PU and NLP-R-SCPM-PU that consider phase uncertainties are better than the other two. The NLP-R-SCPM-PU criterion gives the highest satisfaction ratio due to its most conservative formulation. And its power consumption is only 0.5 dB higher than the SDP-R-SCPM-PU one. In addition, the more robust formulations of SDP-R-SCPM-PU and NLP-R-SCPM-PU make them less sensitive to the value of κ, for which a higher value implies a lower power consumption, and thus a looser protection against ISI. The satisfaction ratio of NLP-R-SCPM-PU is still around 70% when $\kappa = 600$, while the SDP-R-SCPM and QCQP-R-SCPM criteria essentially do not work under this setting. In the following simulations, we set a lower bound $\kappa = 100$ for both κ_p and $\widetilde{\kappa}_p$.

Fig. 8 shows the performance versus ε when $\gamma_0 = 15$ dB. To verify the effectiveness of robust schemes, the satisfaction ratios of the DP scheme in (35) are also provided in the left plot, denoted by DP-SDP and DP-NLP, respectively, when their powers are scaled up to that of SDP-R-SCPM-PU (33) and NLP-R-SCPM-PU (40). Clearly, satisfaction ratios improve when more powers are used to combat larger phase uncertainties. However, the powers increase dramatically if $\varepsilon \geq 5^\circ$. For comparison, the power of SCPM-PU (21) that has the perfect knowledge of phase uncertainties is also shown in the plot. In contrast to SDP-R-SCPM-PU, the largest tolerable ε for NLP-R-SCPM-PU is 1° less if the maximum power is limited to 5 dBm [8]. Judging from these results, a reasonably good performance can be achieved with the proposed robust HBF schemes if $\varepsilon \leq 5.5^\circ$, which is a valid assumption according to the design in [8].

The sum powers and the satisfaction ratios of the NLP-R-SCPM-PU criterion are shown in Table II for $(x_T, z_T) = (5, 1)$, $(x_1, z_1) = (7, 5)$ and user 2 in different locations of the room in Fig. 1. The target SINR is set to 15 dB with $\varepsilon = 3^\circ$ and the lower bound κ for $\widetilde{\kappa}_1$ and $\widetilde{\kappa}_2$ is 100. The values in each

TABLE II
POWER CONSUMPTIONS AND SINR SATISFACTION RATIOS OF THE NLP-R-SCPM-PU CRITERION.

dBm/$\frac{1}{1000}$	z_2 2	3	4	5	6	7	8	9
0	3.5/301	3.7/478	3.6/548	3.9/732	3.2/819	1.6/867	1.0/928	1.6/869
1	2.4/347	2.5/537	2.6/680	1.8/837	-0.1/892	-0.3/957	0.9/960	2.7/930
2	1.4/456	1.2/659	0.4/825	-2.0/933	-1.4/979	0.9/995	3.3/990	5.0/992
3	0.1/561	-1.0/840	-3.8/958	-1.2/918	1.9/976	3.3/999	4.1/910	5.0/540
x_2 4	-2.2/862	-3.3/974	0.3/974	1.3/978	2.5/927	3.5/888	4.4/905	5.1/909
5	-0.7/868	-0.1/849	0.6/807	1.5/749	2.5/769	3.4/754	4.3/839	5.1/825
6	-0.9/654	Inf/-	Inf/-	3.4/480	2.1/346	3.5/348	5.2/423	6.5/473
7	0.3/239	0.3/615	Inf/-	Inf/-	Inf/-	Inf/-	Inf/-	7.1/161
8	0.8/183	3.2/324	1.7/487	Inf/-	Inf/-	Inf/-	Inf/-	Inf/-
9	2.0/222	2.7/239	5.0/329	3.1/340	Inf/-	Inf/-	Inf/-	Inf/-

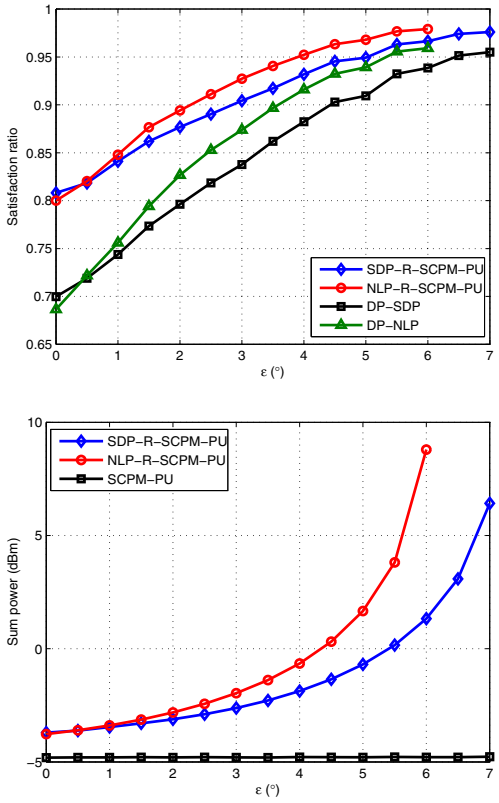

Fig. 8. SINR satisfaction ratios and power consumptions versus ε when $\gamma_0 = 15$ dB and $\kappa = 100$.

entry give the average transmit power in dBm and the total times in which the SINR constraint is satisfied out of 1000 simulation runs when user 2 is in the corresponding location of Fig. 1(b). In some entries, the values are denoted by "Inf/-", which mean the NLP-R-SCPM-PU scheme is infeasible in the corresponding locations, namely, the transmit powers become infinite. This problem is particularly pronounced when user 2 comes in the LOS direction from the transmitter to user 1. As long as the RAFs, (*c.f.* Fig. 3), of user 2 do not highly overlap with the RAF of user 1, for example the space in the upper half of the room, *i.e.* $x < 5$, the satisfaction ratios are greater than 80%. Otherwise the satisfaction ratios decrease dramatically, and the transmit power is relatively higher even if the NLP-R-SCPM-PU scheme is feasible. We note that the performance in space corresponding to the upper and lower left corners of the Table is limited by the antenna gain, $|E(\phi, \theta)|$, of the patch antenna whose values drop by about 30% from its maximum at $\theta = 0°$ as shown in Fig. 3, making it difficult to maintain the SINR.

VII. CONCLUSIONS

We studied time-domain HBF methods for PAA to maintain the received SINR under MAI, ISI and phase uncertainties. The proposed methods only require the transmit directions and RSSIs of the intended users. According to our simulations, phase uncertainties appear to have a dominant impact on system performance. The robustness designed to combat phase uncertainties can help mitigate MAI as well, giving 10% increase in the SINR satisfaction ratio with $1 \sim 2$ dB more power consumption. Under a maximum of 5 dBm transmit power and 3° phase errors, the design objective can be satisfied for 80% of the chances or more with the NLP-R-SCPM-PU criterion as long as users' RAF patterns do not highly overlap with each other. In more general operating scenarios, the maximum acceptable uncertainty is 5.5°, which meet the PAA design in [8]. The proposed HBF schemes can thus be directly applied to SC-FDE, or to OFDM, as well, in which the performance can be further improved if the frequency-domain CSI of each user can be fed back to design frequency-domain precoders, making use of the concept of MU-MIMO.

APPENDIX

The Lagrangian for (40) is given by

$$\mathcal{L} = \sum_{p=1}^{K} \|\mathbf{w}_p\|^2 - \sum_{k=1}^{K} \tau_{p,k} \mathbf{w}_k^\dagger (\nu_{p,k}^2 \|\mathbf{g}_{p,0}\|^2 \mathbf{I} - \mathbf{g}_{p,0}\mathbf{g}_{p,0}^\dagger)\mathbf{w}_k - \lambda_p \left(\frac{1}{\gamma_0} \mathbf{w}_p^\dagger \mathcal{Q}_{p,p} \mathbf{w}_p - \sum_{q \neq p}^{K} \mathbf{w}_q^\dagger \mathcal{Q}_{p,q} \mathbf{w}_q - \frac{\sigma_p^2}{\mathcal{L}_{p,0}} \right) \quad (48)$$

where $\xi_{p,p} \triangleq \epsilon_p(\epsilon_p - 2\nu_{p,p}\|\mathbf{g}_{p,0}\|)$, $\xi_{p,q} \triangleq \epsilon_p(\epsilon_p + 2\nu_{p,q}\|\mathbf{g}_{p,0}\|)$, $\mathcal{Q}_{p,p} \triangleq \mathbf{g}_{p,0}\mathbf{g}_{p,0}^\dagger + \xi_{p,p}\mathbf{I}$ and $\mathcal{Q}_{p,q} \triangleq \mathbf{g}_{p,0}\mathbf{g}_{p,0}^\dagger + (\xi_{p,q} + \frac{\widetilde{\mathcal{K}}_p}{\mathcal{L}_{p,0}})\mathbf{I}$, $p \neq q$, $\forall p, q \in \mathcal{I}_K$. The Karush-Kuhn-Tucker (K.K.T.) conditions [28] for $\mathbf{w}_p$ and $\nu_{p,q}$, and the corresponding dual variables λ_p and $\tau_{p,q}$ follow:

1) Feasibility: For all $p, q \in \mathcal{I}_K$,

$$\begin{aligned} &\tfrac{1}{\gamma_0} \mathbf{w}_p^\dagger \mathcal{Q}_{p,p} \mathbf{w}_p - \sum_{q \neq p}^{K} \mathbf{w}_q^\dagger \mathcal{Q}_{p,q} \mathbf{w}_q - \tfrac{\sigma_p^2}{\mathcal{L}_{p,0}} \geq 0, \\ &\nu_{p,q}^2 \|\mathbf{g}_{p,0}\|^2 \|\mathbf{w}_q\|^2 - |\mathbf{g}_{p,0}^\dagger \mathbf{w}_q|^2 \geq 0, \\ &\lambda_p \geq 0, \ \tau_{p,q} \geq 0. \end{aligned} \quad (49)$$

2) Complementary slackness: For all $p, q \in \mathcal{I}_K$,

$$\begin{aligned} &\tfrac{1}{\gamma_0}\mathbf{w}_p^\dagger \mathcal{Q}_{p,p}\mathbf{w}_p - \sum_{q\neq p}^{K} \mathbf{w}_q^\dagger \mathcal{Q}_{p,q}\mathbf{w}_q = \tfrac{\sigma_p^2}{\mathcal{L}_{p,0}} \\ &\text{or } \lambda_p = 0 \end{aligned} \tag{50}$$

$$\begin{aligned} &|\mathbf{g}_{p,0}^\dagger \mathbf{w}_q|^2 = \nu_{p,q}^2 \|\mathbf{g}_{p,0}\|^2 \|\mathbf{w}_q\|^2 \\ &\text{or } \tau_{p,q} = 0. \end{aligned} \tag{51}$$

3) Zero derivative: The zero-derivative conditions of $\frac{\partial \mathcal{L}}{\partial \nu_{p,q}} = 0$, $\forall p, q \in \mathcal{I}_K$, yield

$$\begin{aligned} \tau_{p,p} &= \frac{1}{\gamma_0}\lambda_p \frac{\epsilon_p}{\nu_{p,p}\|\mathbf{g}_{p,0}\|} \\ \tau_{p,q} &= \lambda_p \frac{\epsilon_p}{\nu_{p,q}\|\mathbf{g}_{p,0}\|},\ p \neq q. \end{aligned} \tag{52}$$

In addition, the zero derivatives *w.r.t.* $\mathbf{w}_p$, $\forall p \in \mathcal{I}_K$, result in

$$\begin{aligned} \tfrac{\partial \mathcal{L}}{\partial \mathbf{w}_p^*} &= \mathbf{w}_p - \tfrac{\lambda_p}{\gamma_0}\mathcal{Q}_{p,p}\mathbf{w}_p + \sum_{q\neq p}^{K} \lambda_q \mathcal{Q}_{q,p}\mathbf{w}_p - \\ &\quad \sum_{k=1}^{K} \tau_{k,p}(\nu_{k,p}^2 \|\mathbf{g}_{k,0}\|^2 \mathbf{I} - \mathbf{g}_{k,0}\mathbf{g}_{k,0}^\dagger)\mathbf{w}_p \\ &= \mathbf{0}. \end{aligned} \tag{53}$$

The K.K.T. conditions from (49) to (53) in general are only the necessary conditions for the optimal primal and dual variables of (40). Supposing that $\nu_{p,q}$ are given, $\forall p, q \in \mathcal{I}_K$, (40) is a QCQP problem in a form that had been shown to be convex in [34]. Therefore, one can expect that [28]

$$\begin{aligned} \tfrac{\partial^2 \mathcal{L}}{\partial \mathbf{w}_p^* \partial \mathbf{w}_p^T} &= \mathbf{I} - \tfrac{\lambda_p}{\gamma_0}\mathcal{Q}_{p,p} + \textstyle\sum_{q\neq p}^{K} \lambda_q \mathcal{Q}_{q,p} - \\ &\quad \sum_{k=1}^{K} \tau_{k,p}(\nu_{k,p}^2 \|\mathbf{g}_{k,0}\|^2 \mathbf{I} - \mathbf{g}_{k,0}\mathbf{g}_{k,0}^\dagger) \succeq \mathbf{0}. \end{aligned} \tag{54}$$

When reformulating (40) as an SDP in $\mathbb{W}_p \triangleq \mathbf{w}_p\mathbf{w}_p^H$, this is also a result of its K.K.T. conditions.

On the other hand, it is easy to show from (48), (51) and (52) that both $\frac{\partial^2 \mathcal{L}}{\partial \nu_{p,p}^2} = \frac{1}{\gamma_0}\lambda_p \epsilon_p \frac{|\mathbf{g}_{p,0}^\dagger \mathbf{w}_p|^2}{\nu_{p,p}^3 \|\mathbf{g}_{p,0}\|} \geq 0$ and $\frac{\partial^2 \mathcal{L}}{\partial \nu_{p,q}^2} = \lambda_p \epsilon_p \frac{|\mathbf{g}_{p,0}^\dagger \mathbf{w}_q|^2}{\nu_{p,q}^3 \|\mathbf{g}_{p,0}\|} \geq 0$, $\forall p, q \in \mathcal{I}_K$, $p \neq q$, given that the feasible optimal $\lambda_p \geq 0$ and $\nu_{p,q} \geq 0$. Therefore, if one can show that $\frac{\partial^2 \mathcal{L}}{\partial \mathbf{w}_p^* \partial \nu_{k,q}} = \mathbf{0}$, $\forall p, k, q \in \mathcal{I}_k$, then $\mathcal{L}$ is convex in $\{\mathbf{w}_p, \nu_{p,q}\}_{p,q=1}^K$ when $\nu_{p,q} > 0$, $\forall p, q \in \mathcal{I}_K$, since we already have $\frac{\partial^2 \mathcal{L}}{\partial \mathbf{w}_p^* \partial \mathbf{w}_q^T} = \mathbf{0}$ by (53), $p \neq q$.

Continued from (53), it follows that $\frac{\partial^2 \mathcal{L}}{\partial \mathbf{w}_p^* \partial \nu_{k,q}} = \mathbf{0}$ when $q \neq p$. Furthermore, we have

$$\frac{\partial^2 \mathcal{L}}{\partial \mathbf{w}_p^* \partial \nu_{p,p}} = 2\left(\frac{\lambda_p}{\gamma_0}\epsilon_p \|\mathbf{g}_{p,0}\| - \tau_{p,p}\nu_{p,p}\|\mathbf{g}_{p,0}\|^2\right)\mathbf{w}_p \tag{55}$$

$$\frac{\partial^2 \mathcal{L}}{\partial \mathbf{w}_p^* \partial \nu_{q,p}} = 2\left(\lambda_q \epsilon_q \|\mathbf{g}_{q,0}\| - \tau_{q,p}\nu_{q,p}\|\mathbf{g}_{q,0}\|^2\right)\mathbf{w}_p \tag{56}$$

which equal zero by (52). Thus, (49) to (53) are the optimal conditions for (40) when $\nu_{p,q} \geq 0$.

From (52), (53) and the definitions of $\mathcal{Q}_{p,p}$ and $\mathcal{Q}_{p,q}$ in (48), it is straightforward to show that

$$\left(\alpha_p \mathbf{I} + \sum_{q\neq p}^{K} \lambda_q \eta_{q,p}\mathbf{g}_{q,0}\mathbf{g}_{q,0}^\dagger\right)\mathbf{w}_p = \frac{\lambda_p}{\gamma_0}\eta_{p,p}\mathbf{g}_{p,0}\mathbf{g}_{p,0}^\dagger \mathbf{w}_p \tag{57}$$

where $\alpha_p \triangleq 1 - \frac{\lambda_p}{\gamma_0}\epsilon_p(\epsilon_p - \nu_{p,p}\|\mathbf{g}_{p,0}\|) + \sum_{q\neq p}^{K} \lambda_q(\epsilon_q(\epsilon_q + \nu_{q,p}\|\mathbf{g}_{q,0}\|) + \frac{\widetilde{\mathcal{K}}_q}{\mathcal{L}_{q,0}})$, $\eta_{p,p} \triangleq 1 - \frac{\epsilon_p}{\|\mathbf{g}_{p,0}\|\nu_{p,p}}$ and $\eta_{q,p} \triangleq 1 + \frac{\epsilon_q}{\|\mathbf{g}_{q,0}\|\nu_{q,p}}$, $\forall p, q \in \mathcal{I}_K$, $q \neq p$. Define $\mathbf{T}_{p,p} \triangleq \alpha_p \mathbf{I} + \sum_{q\neq p}^{K} \lambda_q \eta_{q,p}\mathbf{g}_{q,0}\mathbf{g}_{q,0}^\dagger$. We have

$$\mathbf{w}_p = \frac{\lambda_p}{\gamma_0}\eta_{p,p}(\mathbf{g}_{p,0}^\dagger \mathbf{w}_p)\mathbf{T}_{p,p}^{-1}\mathbf{g}_{p,0}. \tag{58}$$

This formulation of $\mathbf{w}_p$ requires a strict feasibility of $\lambda_p > 0$, $\forall p \in \mathcal{I}_K$, otherwise we have $\mathbf{w}_p = \mathbf{0}$. Consequently by (52), $\tau_{p,q} > 0$, as well, $\forall p, q \in \mathcal{I}_K$. According to (58), we then have $\|\mathbf{w}_p\|^2 = \frac{\lambda_p^2}{\gamma_0^2}\eta_{p,p}^2 |\mathbf{g}_{p,0}\mathbf{w}_p|^2 \mathbf{g}_{p,0}^\dagger \mathbf{T}_{p,p}^{-2}\mathbf{g}_{p,0}$. By the complementary slackness of $|\mathbf{g}_{p,0}^\dagger \mathbf{w}_p|^2 = \nu_{p,p}^2 \|\mathbf{g}_{p,0}\|^2 \|\mathbf{w}_p\|^2$ in (51), we thus obtain

$$\frac{1}{\nu_{p,p}} = \frac{\lambda_p}{\gamma_0}\eta_{p,p}\|\mathbf{g}_{p,0}\| \left\|\mathbf{T}_{p,p}^{-1}\mathbf{g}_{p,0}\right\| \tag{59}$$

given that $\nu_{p,p} \geq 0$, $\lambda_p \geq 0$ and $\eta_{p,p} = 1 - \frac{\epsilon_p}{\|\mathbf{g}_{p,0}\|\nu_{p,p}} \geq 0$ as $\nu_{p,p}\|\mathbf{g}_{p,0}\|\|\mathbf{w}_p\| \geq |\mathbf{g}_{p,0}^\dagger \mathbf{w}_p| \geq \epsilon_p \|\mathbf{w}_p\|$ by (36) and (37). Similarly from (57), we obtain an alternative expression of $\mathbf{w}_p$ given by

$$\begin{aligned} \mathbf{w}_p = -\lambda_q \eta_{q,p}(\mathbf{g}_{q,0}^\dagger \mathbf{w}_p)(\alpha_p \mathbf{I} + \sum_{k\neq p,q}^{K} \lambda_k \eta_{k,p}\mathbf{g}_{k,0}\mathbf{g}_{k,0}^\dagger - \\ \tfrac{\lambda_p}{\gamma_0}\eta_{p,p}\mathbf{g}_{p,0}\mathbf{g}_{p,0}^\dagger)^{-1}\mathbf{g}_{q,0}. \end{aligned} \tag{60}$$

Let $\mathbf{T}_{q,p} \triangleq \alpha_p \mathbf{I} + \sum_{k\neq p,q}^{K} \lambda_k \eta_{k,p}\mathbf{g}_{k,0}\mathbf{g}_{k,0}^\dagger - \frac{\lambda_p}{\gamma_0}\eta_{p,p}\mathbf{g}_{p,0}\mathbf{g}_{p,0}^\dagger$. Since $\lambda_q \geq 0$ and $\eta_{q,p} = 1 + \frac{\epsilon_q}{\|\mathbf{g}_{q,0}\|\nu_{q,p}} \geq 0$, together with the complementary slackness of $|\mathbf{g}_{q,0}^\dagger \mathbf{w}_p|^2 = \nu_{q,p}^2 \|\mathbf{g}_{q,0}\|^2 \|\mathbf{w}_p\|^2$ in (51), it follows

$$\frac{1}{\nu_{q,p}} = \lambda_q \eta_{q,p}\|\mathbf{g}_{q,0}\| \left\|\mathbf{T}_{q,p}^{-1}\mathbf{g}_{q,0}\right\|, \forall q \neq p. \tag{61}$$

Since α_p, and, hence, $\mathbf{T}_{q,p}$ are also functions of $\nu_{p,p}$ and $\nu_{q,p}$, $\forall p, q \in \mathcal{I}_K$, the values of $\nu_{p,p}$ and $\nu_{q,p}$ can thus be solved iteratively from (59) and (61) with the fixed-point method, given λ_p. Recall from (37) that $|\mathbf{g}_{p,0}^\dagger \mathbf{w}_p| \geq \epsilon_p \|\mathbf{w}_p\|$ which implies $\nu_{p,p} \geq \frac{\epsilon_p}{\|\mathbf{g}_{p,0}\|}$ due to $|\mathbf{g}_{p,0}^\dagger \mathbf{w}_p| \leq \nu_{p,p}\|\mathbf{g}_{p,0}\|\|\mathbf{w}_p\|$ by (36). In addition, by the Cauchy-Schwartz inequality, we have $|\mathbf{g}_{q,0}^\dagger \mathbf{w}_p|^2 \leq \|\mathbf{g}_{q,0}\|^2 \|\mathbf{w}_p\|^2$, thus $\nu_{q,p} \leq 1$, $\forall p, q \in \mathcal{I}_K$, according to the definition of (36). Together with the constraints of $\nu_{q,p} \geq 0$, we obtain the feasible searching range for $\nu_{q,p}$ given by

$$\frac{\epsilon_p}{\|\mathbf{g}_{p,0}\|} \leq \nu_{p,p} \leq 1, \quad 0 \leq \nu_{q,p} \leq 1, \ \ p, q \in \mathcal{I}_K,\ p \neq q. \tag{62}$$

The expressions of $\nu_{p,p}$ and $\nu_{q,p}$ in (59) and (61) are functions of λ_p. In the sequel, we will show that λ_p can also be expressed as a function of $\nu_{p,p}$ and $\nu_{q,p}$, which leads to an iterative algorithm for solving $\nu_{p,p}$, $\nu_{q,p}$ and λ_p in the feasible ranges of $\nu_{p,p}$ and $\nu_{q,p}$ in (62) and $\lambda_p > 0$.

Continued from (58), multiplying both sides by $\mathbf{g}_{p,0}^{\dagger}$ and having $\mathbf{g}_{p,0}^{\dagger}\mathbf{w}_p \neq 0$ results in

$$\frac{1}{\lambda_p} = \frac{1}{\gamma_0}\eta_{p,p}\mathbf{g}_{p,0}^{\dagger}\mathbf{T}_{p,p}^{-1}\mathbf{g}_{p,0} \tag{63}$$

which can also be solved by the fixed-point method, given $\nu_{p,q}, \forall p,q \in \mathcal{I}_K$, since $\mathbf{T}_{p,p}$ is a function of λ_p as well. The convergence of (63), given $\nu_{p,q}, \forall p,q \in \mathcal{I}_K$, can be proven following the procedure in Appendix II of [34]. Therefore, if fixed points of (59) and (61) exist in the ranges of (62), then $\widehat{\mathbf{w}}_p$ can be continued to solve from the conditions of (50) and (58). Without the loss of generality, we can have $\chi_p \triangleq \mathbf{g}_{p,0}^{\dagger}\mathbf{w}_p$ to be positive reals and rewrite (58) as

$$\mathbf{w}_p = \frac{\lambda_p}{\gamma_0}\eta_{p,p}\mathbf{T}_{p,p}^{-1}\mathbf{g}_{p,0}\chi_p. \tag{64}$$

Substituting this expression of $\mathbf{w}_p$ back into (50) followed by some mathematical manipulations, one can easily show that $\mathbf{F}\Gamma = \Upsilon$, with $\Gamma \triangleq [\chi_1^2, \ldots, \chi_K^2]^T$, $\Upsilon \triangleq [\frac{\sigma_1^2}{\mathcal{L}_{1,0}}, \ldots, \frac{\sigma_K^2}{\mathcal{L}_{K,0}}]^T$, and the entries of $\mathbf{F}$ given by

$$F_{p,p} \triangleq \frac{\lambda_p^2}{\gamma_0^3}\eta_{p,p}^2\left(\left|\mathbf{g}_{p,0}^{\dagger}\mathbf{T}_{p,p}^{-1}\mathbf{g}_{p,0}\right|^2 + \xi_{p,p}\left\|\mathbf{T}_{p,p}^{-1}\mathbf{g}_{p,0}\right\|^2\right) \tag{65}$$

$$F_{p,q} \triangleq -\frac{\lambda_q^2}{\gamma_0^2}\eta_{q,q}^2\left(\left|\mathbf{g}_{p,0}^{\dagger}\mathbf{T}_{q,q}^{-1}\mathbf{g}_{q,0}\right|^2 + \xi_{p,q}\left\|\mathbf{T}_{q,q}^{-1}\mathbf{g}_{q,0}\right\|^2\right) \tag{66}$$

$p,q \in \mathcal{I}_K,\ p \neq q$. Suppose that $\mathbf{F} \succ \mathbf{0}$, then there exist positive real solutions of χ_p. Substituting the resultant χ_p back into (64) gives the optimal $\widehat{\mathbf{w}}_p$. Finally, by (53) and (51), we have $\widehat{\mathbf{w}}_p^{\dagger}\widehat{\mathbf{w}}_p - \frac{\lambda_p}{\gamma_0}\widehat{\mathbf{w}}_p^{\dagger}\mathcal{Q}_{p,p}\widehat{\mathbf{w}}_p + \sum_{q\neq p}^{K}\lambda_q\widehat{\mathbf{w}}_p^{\dagger}\mathcal{Q}_{q,p}\widehat{\mathbf{w}}_p = 0$. Substituting this condition back into (48), and employing the complementary slackness of (51) give the optimal objective value : $\sum_{p=1}^{K}\lambda_p\frac{\sigma_p^2}{\mathcal{L}_{p,0}}$.

REFERENCES

[1] "IEEE 802.15 WPAN Millimeter Wave Alternative PHY Task Group (TG3c)." Available: http://www.ieee802.org/15/pub/TG3c.html.

[2] "WirelessHD." Available: http://www.wirelesshd.org/index.html.

[3] "IEEE 802.11ad: Very High Throughput 60 GHz." Available: http://www.ieee802.org/11/.

[4] "WiGig White Paper: Defining the Future of Multi-Gigabit Wireless Communications," July 2010. Available: http://wirelessgigabitalliance.org/specifications/.

[5] H. Yang, P. F. M. Smulders, and I. Akkermans, "On the design of low-cost 60-GHz radios for multigigabit-per-second transmission over short distances," *IEEE Commun. Mag.*, vol. 45, no. 12, pp. 44–51, Dec. 2007.

[6] C. R. Anderson and T. S. Rappaport, "In-building wideband partition loss measurements at 2.5 and 60 GHz," *IEEE Trans. Commun.*, vol. 3, no. 3, pp. 922–928, May 2004.

[7] C. H. et. al., "NT-11 beamforming introduction," IEEE 802.11-10/0430r1.doc, May 2010. Available: http://mentor.ieee.org/802.11/dcn/11/11-10-0430-01-00ad-nt-11.ppt.

[8] A. Valdes-Garcia, S. T. Nicolson, J.-W. Lai, A. Natarajan, P.-Y. Chen, S. K. Reynolds, J.-H. C. Zhan, D. G. Kam, D. Liu, and B. Floyd, "A fully integrated 16-element phased-array transmitter in SiGe BiCMOS for 60-GHz communications," *IEEE J. Solid-State Circuits*, vol. 45, no. 12, pp. 2757–2773, Dec. 2010.

[9] E. Cohen, C. Jakobson, S. Ravid, and D. Ritter, "A thirty two element phased-array transceiver at 60GHz with RF-IF conversion block in 90nm flip chip CMOS process," in *Proc. 2010 IEEE Radio Frequency Integrated Circuits Symp.*

[10] M. Tabesh, J. Chen, C. Marcu, L. Kong, S. Kang, A. M. Niknejad, and E. Alon, "A 65 nm CMOS 4-element Sub-34 mW/element 60 GHz phased-array transceiver," *IEEE J. Solid-State Circuits*, vol. 46, no. 12, pp. 3018–3032, Dec. 2011.

[11] S.-H. Wu, L.-K. Chiu, K.-Y. Lin, and S.-J. Chung, "Planar arrays hybrid beamforming for SDMA in millimeter wave applications," in *Proc. 2008 IEEE International Symp. Personal, Indoor Mobile Radio Commun.*

[12] C. Yiu and S. Singh, "Empirical capacity of mmWave WLANs," *IEEE J. Sel. Areas Commun.*, vol. 27, no. 8, pp. 1479–1487, Oct. 2009.

[13] S.-H. Wu, K.-Y. Lin, and L.-K. Chiu, "Hybrid beamforming using convex optimization for SDMA in millimeter wave radio," in *Proc. 2009 IEEE PIMRC.*

[14] ——, "Hybrid beamforming for two-user SDMA in millimeter wave radio," in *Proc. 2010 IEEE PIMRC.*

[15] X. Huang, Y. J. Guo, and J. D. Bunton, "A hybrid adaptive antenna array," *IEEE Trans. Wireless Commun.*, vol. 9, no. 5, pp. 1770–1779, May 2010.

[16] E. Torkildson, U. Madhow, and M. Rodwell, "Indoor millimeter wave MIMO: feasibility and performance," *IEEE Trans. Wireless Commun.*, vol. 10, no. 12, pp. 4150–4160, Dec. 2011.

[17] J. Nsenga, A. Bourdoux, and F. Horlin, "Mixed analog/digital beamforming for 60GHz MIMO frequency selective channels," in *Proc. 2010 IEEE International Conf. Commun.*

[18] J. Nsenga, A. Bourdoux, W. V. Thillo, V. Ramon, and F. Horlin, "Joint TX/RX analog linear transformation for maximizing the capacity at 60 GHz," in *Proc. 2011 IEEE ICC.*

[19] A. Arvanitis, G. Anagnostou, N. Moraitis, and P. Constantinou, "Capacity study of a multiple element antenna configuration in an indoor wireless channel at 60GHz," in *Proc. 2007 IEEE Veh. Technol. Conf. – Spring*.

[20] H. Yang, P. F. M. Smulders, and M. H. A. J. Herben, "Channel characteristics and transmission performance for various channel configurations at 60 GHz," *EURASIP J. Wireless Commun. Netw.*, 2007.

[21] J. Wang, Z. Lan, C.-W. Pyo, T. Baykas, C.-S. Sum, M. A. Rahman, R. Funada, F. Kojima, I. Lakkis, H. Harada, and S. Kato, "Beam codebook based beamforming protocol for multi-Gbps millimeter-wave WPAN systems," *IEEE J. Sel. Areas Commun.*, vol. 27, no. 8, pp. 1390–1399, Oct. 2009.

[22] H.-L. Chao and M.-P. Hsu, "CTAP-Minimized scheduling algorithm for millimeter wave based wireless personal area networks," *IEEE Trans. Veh. Technol.*, vol. 60, no. 8, pp. 3840–3852, Oct. 2011.

[23] M. X. Gong, D. Akhmetov, R. Want, and S. Mao, "Multi-user operation in mmWave wireless networks," in *Proc. 2011 IEEE ICC*.

[24] V. Venkateswaran and A.-J. van der Veen, "Analog beamforming in MIMO communications with phase shift networks and online channel estimation," *IEEE Trans. Signal Process.*, vol. 58, no. 8, pp. 4131–4143, Aug. 2010.

[25] D. Falconer, S. L. Ariyavisitakul, A. Benyamin-Seeyar, and B. Eidson, "Frequency domain equalization for single-carrier broadband wireless systems," *IEEE Commun. Mag.*, vol. 40, no. 4, pp. 58–66, Apr. 2002.

[26] S. Kato, H. Harada, R. Funada, T. Baykas, C. S. Sum, J. Wang, and M. A. Rahman, "Single carrier transmission for multi-gigabit 60-GHz WPAN systems," *IEEE J. Sel. Areas Commun.*, vol. 27, no. 8, pp. 1466–1478, Oct. 2009.

[27] K. R. Carver, W. K. Cooper, and W. L. Stutzman, "Beam-pointing errors of planar-phased arrays," *IEEE Trans. Antennas Propagation*, vol. 21, no. 2, pp. 199–202, Mar. 1973.

[28] S. Boyd and L. Vandeberghe, *Convex Optimization*. Cambridge University Press, 2004.

[29] C. A. Balanis, *Antenna Theory*, 2nd ed. John Wiley & Sons, 1997.

[30] H. Vettikalladi, L. L. Coq, O. Lafond, and M. Himdi, "High efficient slot coupled superstrate antenna for 60GHz WLAN applications," in *Proc. 2010 European Conf. Antennas Propagation.*

[31] P. F. M. Smulders, "Statistical characterization of 60-GHz indoor radio channels," *IEEE Trans. Antennas Propag.*, vol. 57, no. 10, pp. 2820–2829, Oct. 2009.

[32] A. M. et al, "Channel Models for 60 GHz WLAN Systems," IEEE doc. 802.11-09/0334r0, 3 2009.

[33] M.-D. Tsai and A. Natarajan, "60GHz passive and active RF-path phase shifters in silicon," in *Proc. 2009 IEEE Radio Frequency Integrated Circuits Symp.*

[34] A. Wiesel, Y. C. Eldar, and S.Shamai, "Linear precoding via conic optimization for fixed MIMO receivers," *IEEE Trans. Signal Process.*, vol. 54, no. 1, pp. 161–176, Jan. 2006.

[35] J. F. Sturm, "Using SeDuMi 1.02, a MATLAB Toolbox for optimization over symmetric cones," *Optimization Methods Software*, vol. 11-12, pp. 625–653, 1999.

[36] M. Grant and S. Boyd, *CVX: Matlab Software for Disciplined Convex Programming (web page and software)*, 2nd ed. Available: http://cvxr.com/cvx.

[37] D. Tse and P. Viswanath, *Fundamentals of Wireless Communication*. Cambridge University Press, 2005.

[38] S.-K. Yong, "TG3c channel modeling sub-committee final report," IEEE 802.15-07-0584-00, Mar. 2007.
[39] M. B. Shebiyda and T. N. Davidson, "Convex conic formulations of robust downlink precoder designs with quality of service constraints," *IEEE J. Sel. Areas Commun.*, vol. 1, no. 4, pp. 714–724, Dec. 2007.
[40] I. Wajid, Y.-C. Eldar, and A. Gershman, "Robust downlink beamforming using covariance channel state information," in *Proc. 2009 IEEE International Conf. Acoustics, Speech Signal Process.*
[41] E. A. Gharavol, Y.-C. Liang, and K. Mouthaan, "Robust downlink beamforming in multiuser MISO cognitive radio networks with imperfect channel-state information," *IEEE Trans. Veh. Technol.*, vol. 59, no. 6, pp. 2852–2860, July 2010.
[42] G. Zheng, K.-K. Wong, and T.-S. Ng, "Robust linear MIMO in the downlink: a worst-case optimization with ellipsoidal uncertainty regions," *EURASIP J. Advances Signal Process.*, vol. 2008, pp. 1–15, June 2008.
[43] T.-H. Chang, W.-K. Ma, and C.-Y. Chi, "Worst-case robust multiuser transmit beamforming using semidefine relaxation: duality and implications," in *Proc. 2011 Asilomar Conf. Signals, Syst., Comput.*
[44] E. de Klerk, *Aspects of Semidefinite Programming: Interior Point Algorithms and Selected Applications*. Kluwer Academic Publishers, 2002.
[45] M. Abramowitz and I. A. Stegun, *Handbook of Mathematical Functions with Formulas, Graphs, and Mathematical Tables*, 9th ed. Dover, 1972.

Sau-Hsuan Wu received the B.S. and the M.S. degrees from National Cheng Kung University, Taiwan in 1990 and 1993, respectively, both in Engineering Science. From 1993 to 1995, he served in the Army of Taiwan, and from 1995 to 1999, he worked as a circuit and system design engineer in Taiwan. In 2003, he received the Ph.D. degree in Electrical Engineering from the University of Southern California, Los Angeles. From 2003 to 2004, he was a postdoctoral research fellow at the Department of Electrical Engineering, University of Southern California, Los Angeles. From 2004 to 2005, he served as a technical consultant for Winbond Electronics Corporation America, developing wireless MIMO-OFDM products. Since 2005, he has been with National Chiao Tung University, Taiwan, and is currently an associated Professor at the Department of Electrical and Computer Engineering. His research interest lies in algorithm designs and performance analysis for wireless communication systems.

Lin-Kai Chiu was born in Hsinchu, Taiwan. He received the B.S. and M.S. degrees in Communications Engineering from National Chiao Tung University (NCTU), Hsinchu, Taiwan, in 2005 and 2007, respectively. Currently, he is a Ph.D. student at the Institute of Communications Engineering, NCTU, Taiwan, and is a member of MBWCL group under supervision of Prof. Sau-Hsuan Wu. His research interest is in MIMO systems and the application of signal processing to millimeter wave systems.

Ko-Yen Lin was born in Taichung, Taiwan. He received the B.S. degree in Communications Engineering from the National Central University, Chung-Li, Taiwan, R.O.C., in 2007, and the M.S. degree in Communications Engineering from National Chiao Tung University, Hsinchu, Taiwan, R.O.C., in 2009. He served as an engineer in MStar Semiconductor, Inc., Hsinchu, Taiwan in 2010. He is currently with the Ministry of Justice, Investigation Bureau, Taiwan. His research interests are in the areas of millimeter wave transmissions, cooperation communications, and convex optimization.

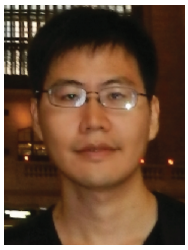

Tsung-Hui Chang (S'07-M'08) received the B.S. degree in electrical engineering and the Ph.D. degree in communications engineering from the National Tsing Hua University (NTHU), Hsinchu, Taiwan, in 2003 and 2008, respectively. Since September 2012, he has been with the Department of Electronic and Computer Engineering, National Taiwan University of Science and Technology (NTUST), Taipei, Taiwan, as an Assistant Professor. Before joining NTUST, he held research positions with NTHU (2008-2011), and University of California at Davis, CA (2011-2012). He was also a visiting scholar of the University of Minnesota, Twin Cities, MN, the Chinese University of Hong Kong and Xidian University, China. His research interests are widely in signal processing problems in wireless communications and smart grid, and convex optimization methods and its applications.